

Limits of existence of light nuclei, ECT\*, Italy, October 2010

## Structure and reactions of selected unstable nuclear systems

A.S. Jensen<sup>a</sup>, D.V. Fedorov<sup>a</sup>, R. De Diego<sup>b</sup>, E. Garrido<sup>b</sup>, R. Álvarez-Rodríguez<sup>c</sup>

<sup>a</sup>Department of Physics and Astronomy, Aarhus University, Denmark

<sup>b</sup>Instituto de Estructura de la Materia, CSIC, Madrid, Spain

<sup>c</sup>Dept. Atom-Mol-Nucl, Universidad Complutense de Madrid, Spain

### CONTENT:

1. Interpretation of topics
2. Concepts and theoretical framework
3. Decay mechanisms of three-body decaying resonances,  $^{12}\text{C}$
4. Systematics of  $^9\text{Be}$ -resonances
5. Dalitz plots: Theory and Measurements
6. Astrophysical rates: Density and temperature dependence
7. Summary and conclusions

## How to understand “Limits of existence”?

Binding energies approaching zero

Resonances with a lifetime, measurable or only theoretical

Continuum states in general

Structure under sea level

In high density or high temperature environments

I choose to include structure and reaction processes

Reactions are un-avoidable to test, measure or infer structure

## Binding energies approaching zero

Halo behavior

Three-body scaling plot

Efimov effect, Borromean systems, etc.

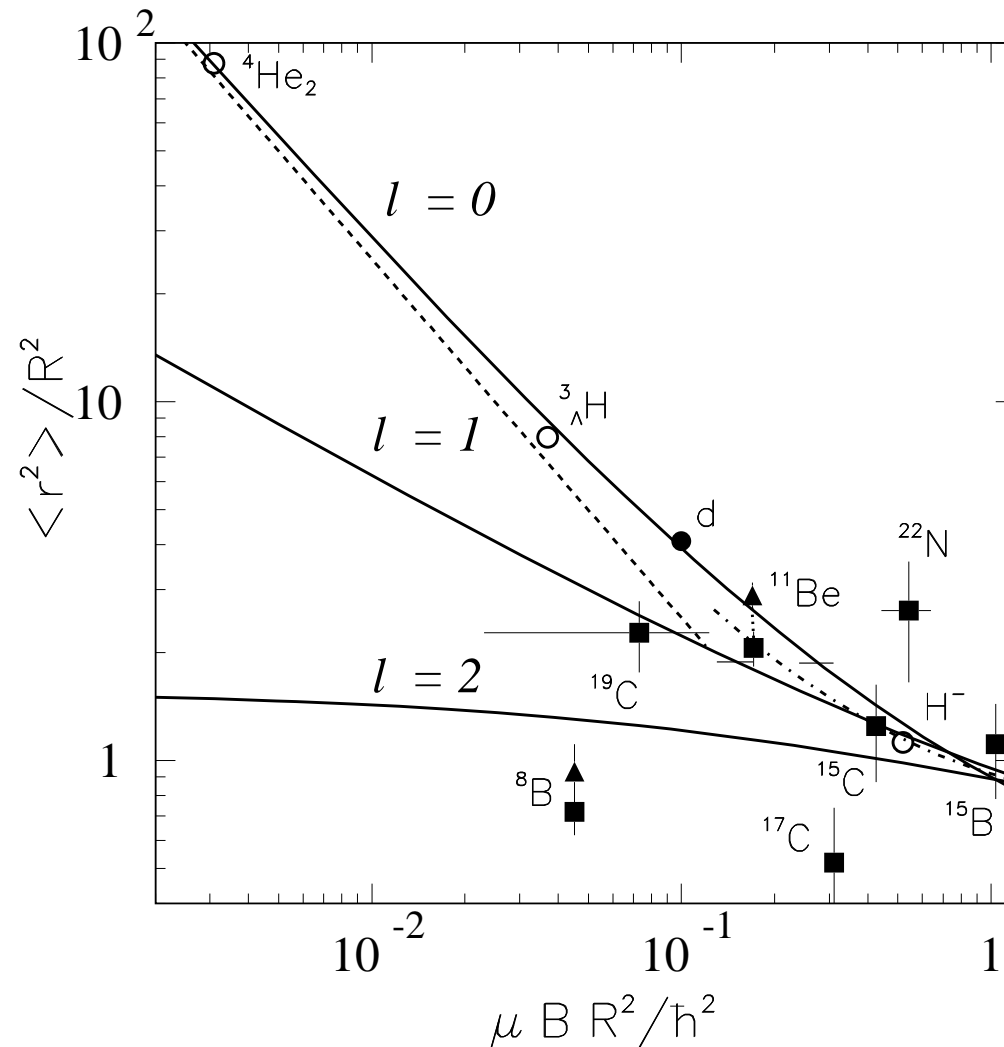


Figure 1: Scaling plot for two-body halos. The ratio of the halo and the potential square radii as function of the scaled separation energy. The dashed line is for an  $s$ -wave Yukawa wave function. The solid and dash-dotted lines are for square-well and  $r^{-2}$ -potentials. The thin horizontal lines indicate where 50% of the wave function is outside the potential. Filled and open symbols are experimental data or from theoretical calculations.

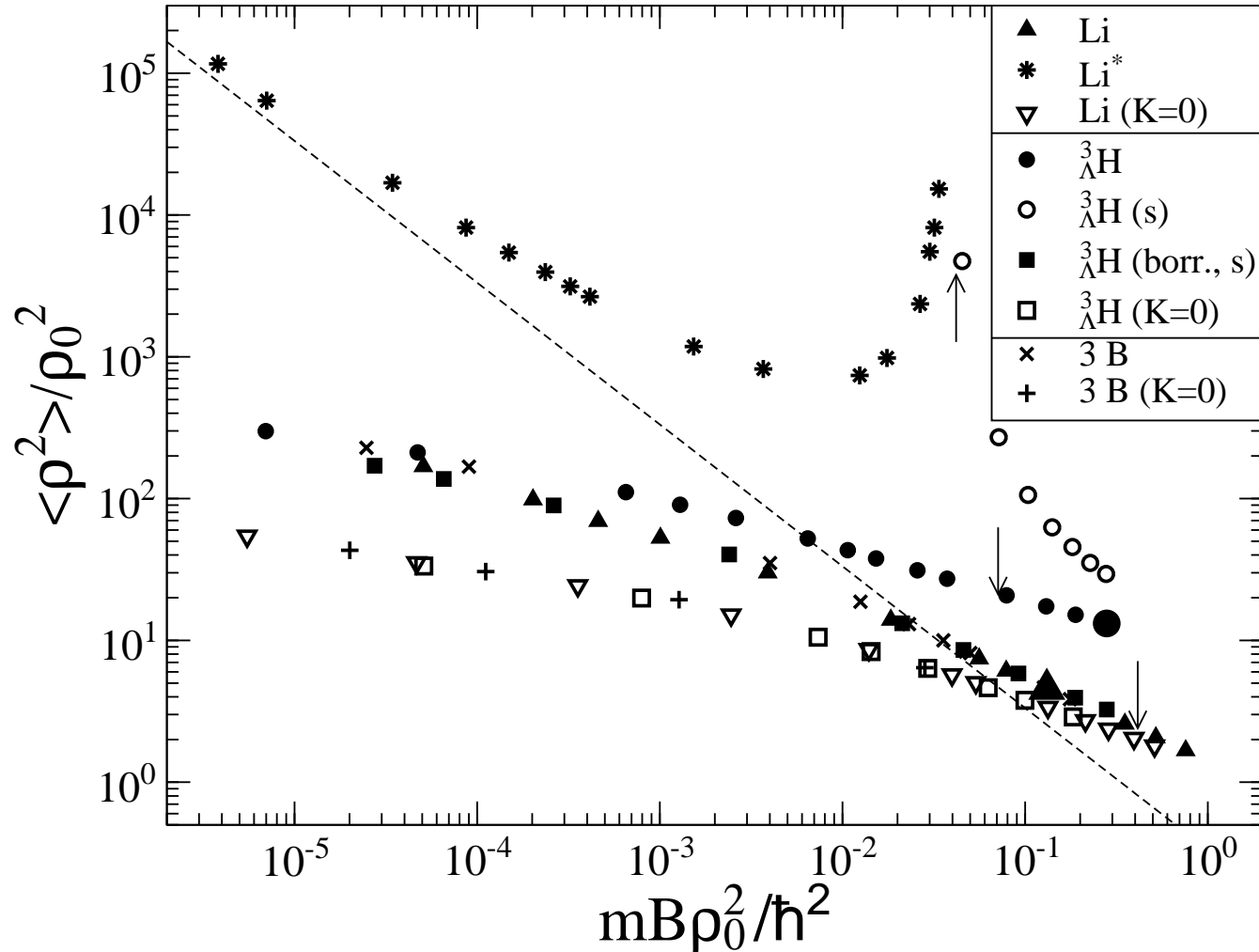


Figure 2: Scaling plot for three-body halos. The dashed line is the Efimov curve for  $\nu = 0$ . Triangles and stars are for masses corresponding to  ${}^{11}\text{Li}$  ( ${}^9\text{Li}+n+n$ ). Squares and circles are for  ${}^3_{\Lambda}H$  ( $\Lambda+n+p$ ). Large closed triangle and square are realistic points. Plus signs and crosses are for three different particles with two scattering lengths while the third is varied. The arrows indicate transitions between Borromean, tango and bound state regions.

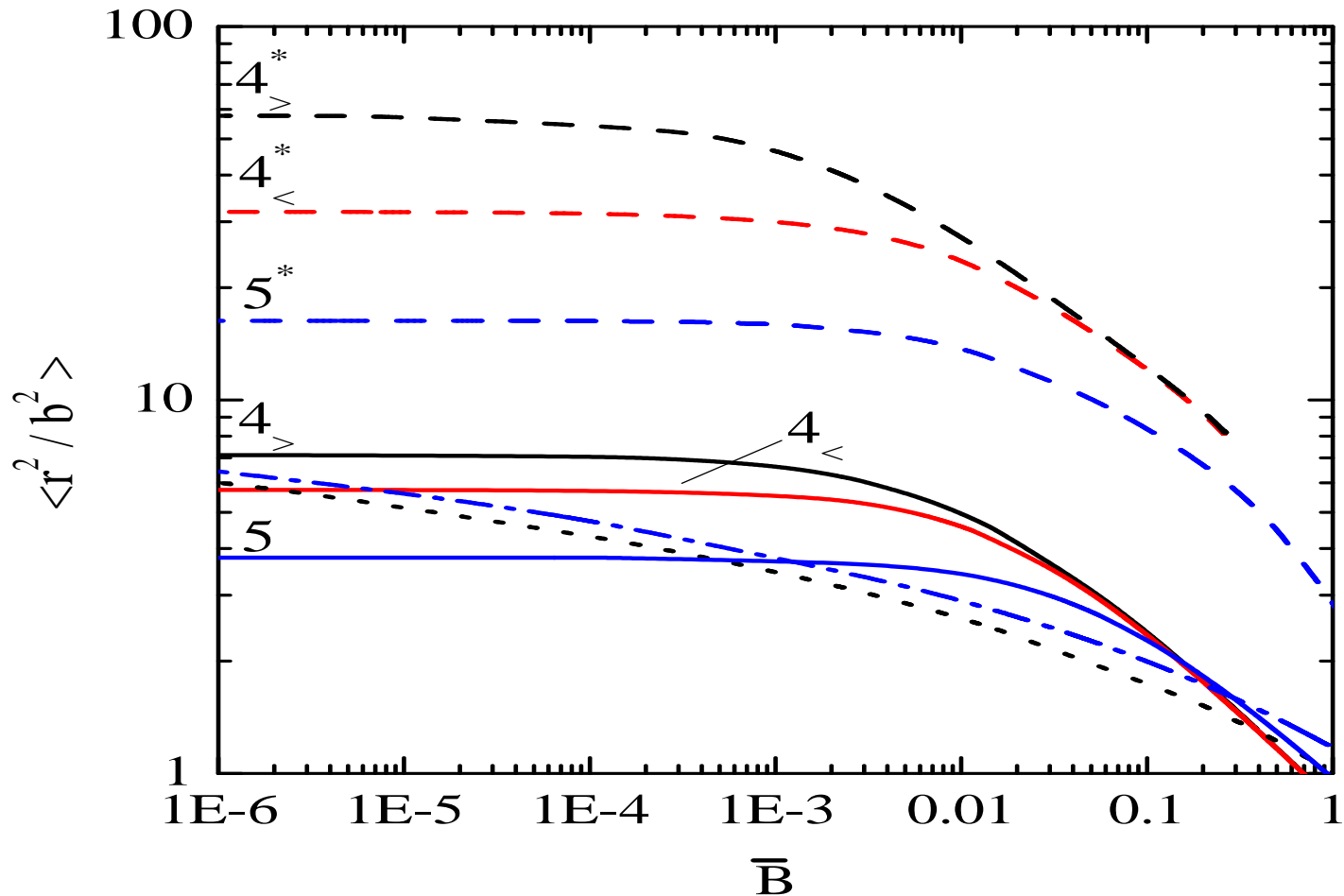


Figure 3: The mean square radius as function of the four and five-body binding energies, all in dimensionless units. The trap sizes for four particles are  $b_t = 230.942a_0$  (red lines with  $4_{<}$ ),  $2630.956a_0$  (black lines with  $4_{>}$ ), and  $b_t = 372.073a_0$  (blue lines with 5) for five particles. Here  $a_0$  is the Bohr radius. We show ground (solid) and excited states (long-dashed with particle numbers tagged with an \*), and “classical” two-body radius (dotted (4) and dot-dashed (5)) translated by Eq.(??).

## Structure under sea level

Outside dripline reefs could appear below the sea

For similar particles outside a core

Core + one particle is unbound the resonance energy  $\varepsilon$

Energy for  $N - 1$  particles is  $E = \varepsilon(N - 1) + v(N - 1)(N - 2)/2$

$v$  is the (negative) potential energy from the pairwise interaction

$E < 0$  when  $\varepsilon < -v(N - 2)/2$

Many particles may add their individually insufficient contribution

Reaching an  $N$ -body BOUND state then seems easy

## **New shell structures, new magic numbers**

Assume a Borromean system of two identical fermions and a core

More fermion pairs would often not lead to unbound systems

Specific numbers of pairs may form configurations of special stability

This is additional quantum stabilization due to special correlations

Magic numbers corresponding to new cluster combinations could arise

Close to threshold a system would correlate to avoid falling apart

At the edge of stability this marginal energy gain may lead to binding

Quantum halos stabilized by new shell structure is a possibility:  
PLB 264 (1991) 238, NPA 537 (1992) 45.

## Theoretical ingredients for three particles

Hyperspherical adiabatic expansion method with hyperradius defined in terms of masses  $m_k$ , particle and centre-of-mass coordinates  $\mathbf{r}_k$  and  $\mathbf{R}$

$$m\rho^2 = \sum_k m_k (\mathbf{r}_k - \mathbf{R})^2 = \frac{1}{m_i + m_k + m_j} \sum_{i < j} m_i m_j \mathbf{r}_{ij}^2$$

The differential equation for one decoupled radial wavefunction is

$$\left[ -\frac{d^2}{d\rho^2} + \frac{\lambda(\rho) + 15/4}{\rho^2} + Q(\rho) - \frac{2mE}{\hbar^2} \right] f(\rho) = 0 ,$$

The total wavefunction  $\psi$  and the diagonal coupling  $Q$  are

$$\psi = \frac{1}{\rho^{5/2}} f(\rho) \phi(\rho, \Omega) , \quad Q(\rho) = \langle \phi | \frac{\partial^2}{\partial \rho^2} | \phi \rangle_{\Omega} ,$$

where the angular coordinates, wavefunction, eigenvalue are  $\Omega, \phi, \lambda$

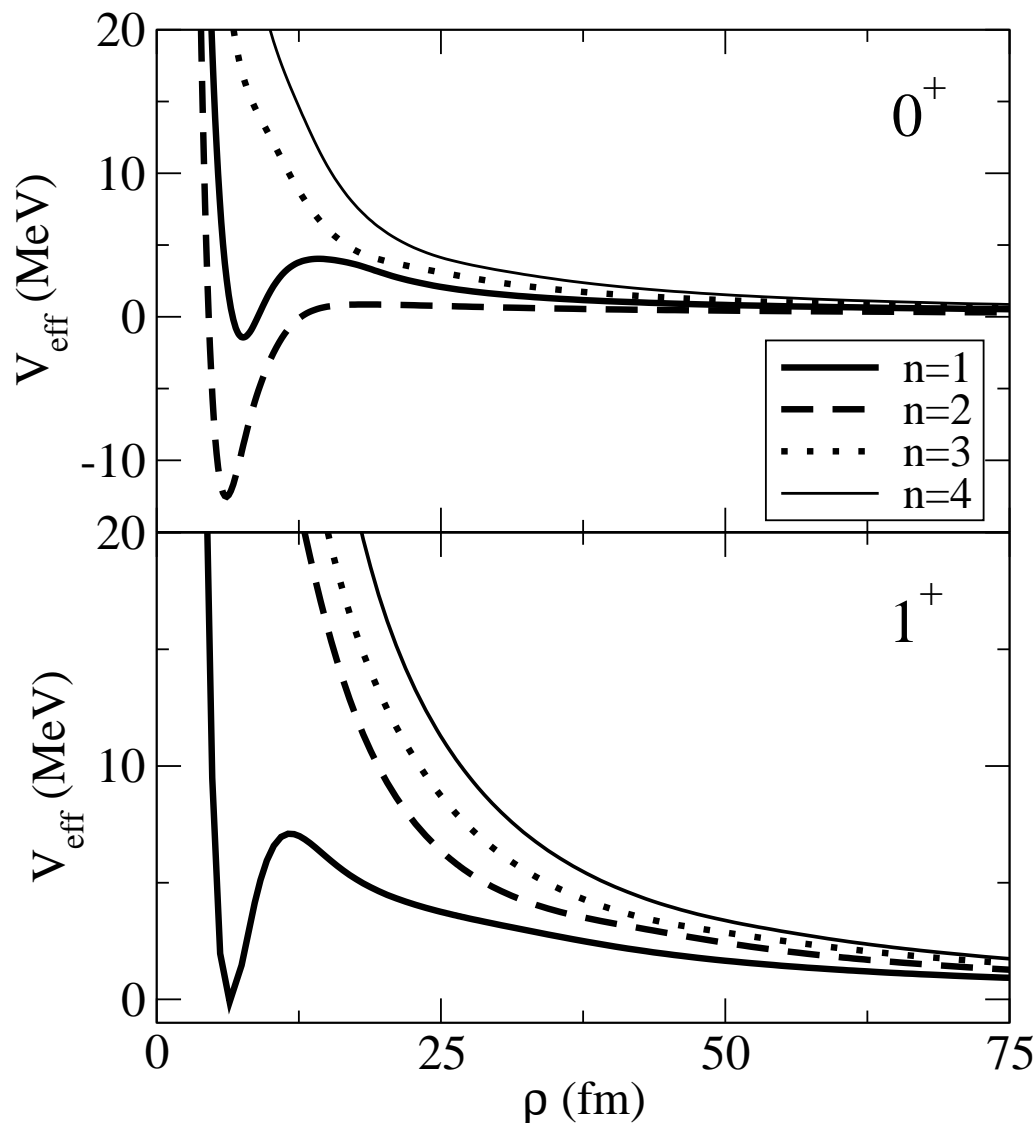


Figure 4: The real parts of the four lowest adiabatic effective potentials, including the three-body potentials, as functions of  $\rho$  for the  $0^+$  and  $1^+$  resonances of  $^{12}\text{C}$ . The two-body interaction is a slightly modified version of the Ali-Bodmer potential. The three-body Gaussian potentials,  $S \exp(-\rho^2/b^2)$ , have  $b = 6$  fm and  $-S = 20, 92$  MeV for  $0^+$  and  $1^+$ , respectively.

## **Effective potentials**

Short-distance is inside clusters, reduce degrees of freedom

Attraction providing bound state or resonance

Barrier providing width

Asymptotic large-distance structure providing momentum distribution

## **Decay mechanism or dynamic evolution**

Sequential through intermediate substructure

Direct into three-body continuum

Dynamic evolution

## Decay mechanism exemplified by $^{12}\text{C}$ states

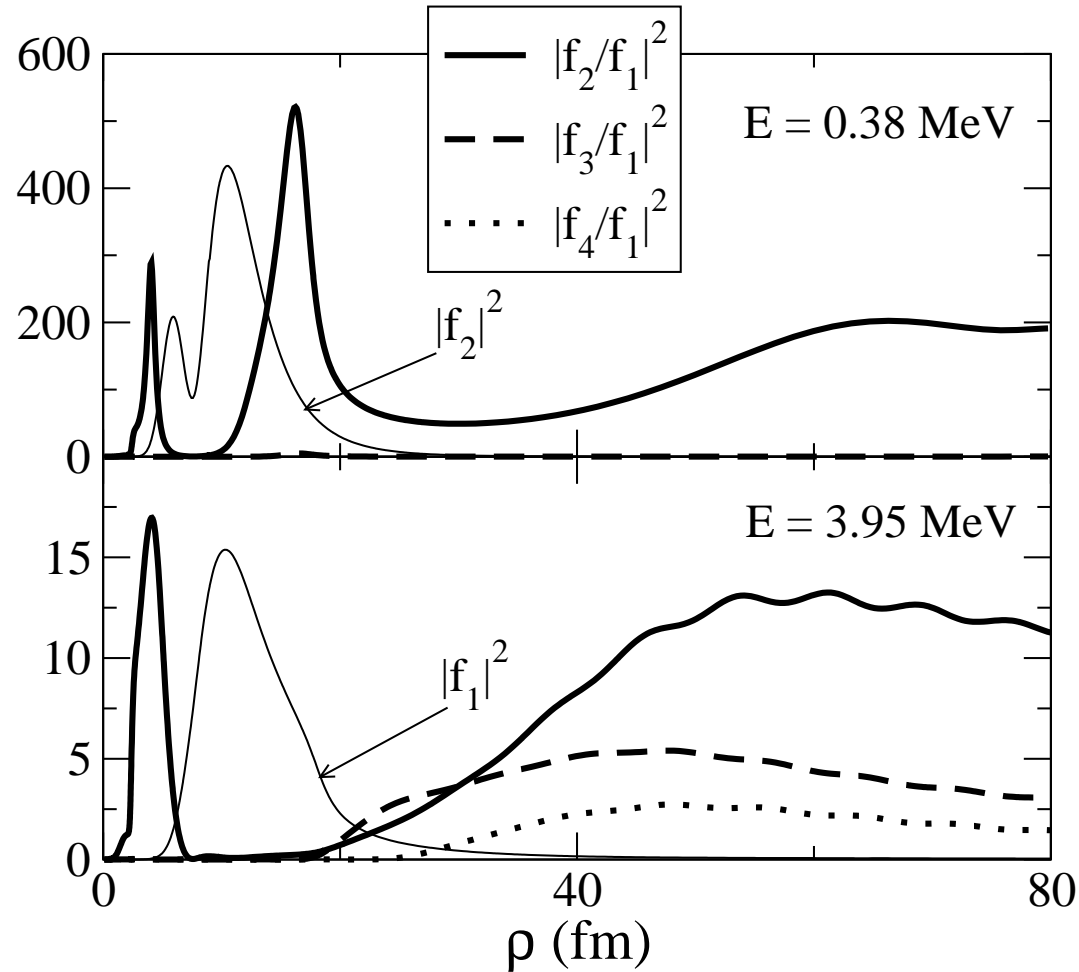


Figure 5: The four lowest radial wavefunctions as functions of  $\rho$  for each of the two  $0^+$ -resonances of  $^{12}\text{C}$  at 0.38 MeV and 3.95 MeV above threshold or at excitation energies of 7.63 MeV and 11.2 MeV. Ratios and the small-distance dominating wavefunctions are given for both states.

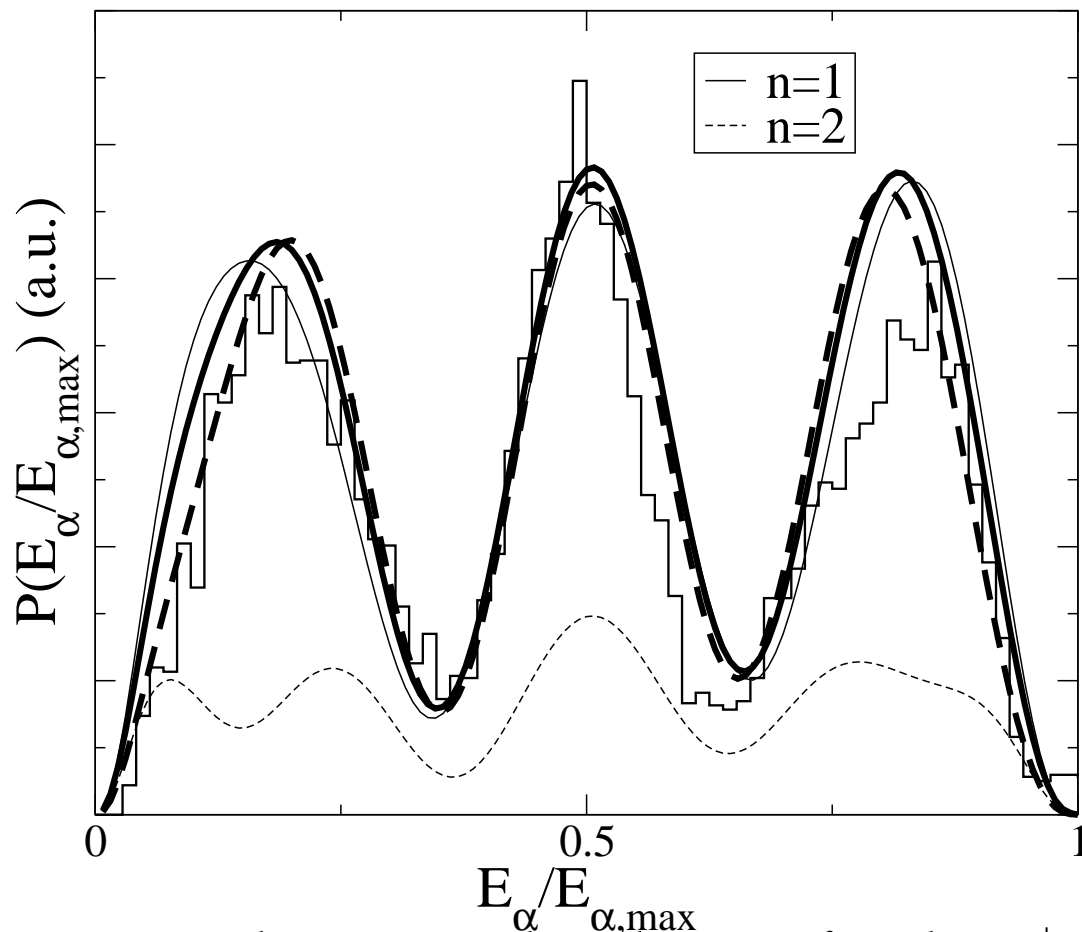


Figure 6: The  $\alpha$ -particle energy distribution for the  $1^+$  resonance of  $^{12}\text{C}$  at 5.43 MeV above threshold at an excitation of 12.71 MeV. The energy is measured in units of the maximum possible, i.e.  $2 \times 5.43/3$  MeV. The thick solid and dashed curves are for coordinate space wavefunctions at  $\rho = 70, 100$  fm. The thin curves are contributions from separate adiabatic potentials. The momentum space computation (described below) fall on top of the  $\rho = 100$  fm curve (thick dashed). The histogram is the experimental distribution from Diget et al..

## The ${}^9\text{Be}(5/2^-)$ -resonance.

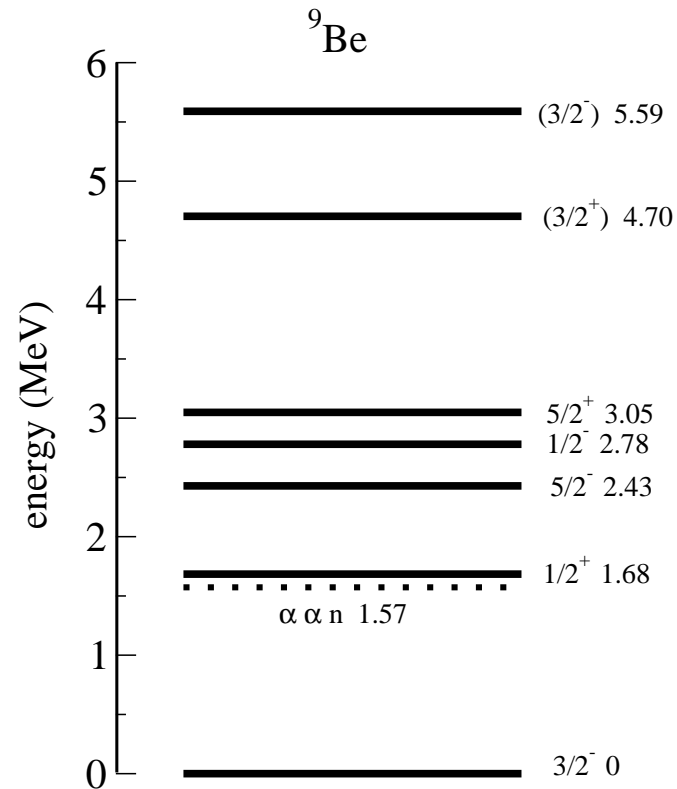


Figure 7: Scheme of the experimentally known levels of  ${}^9\text{Be}$  below 6 MeV of excitation energy.

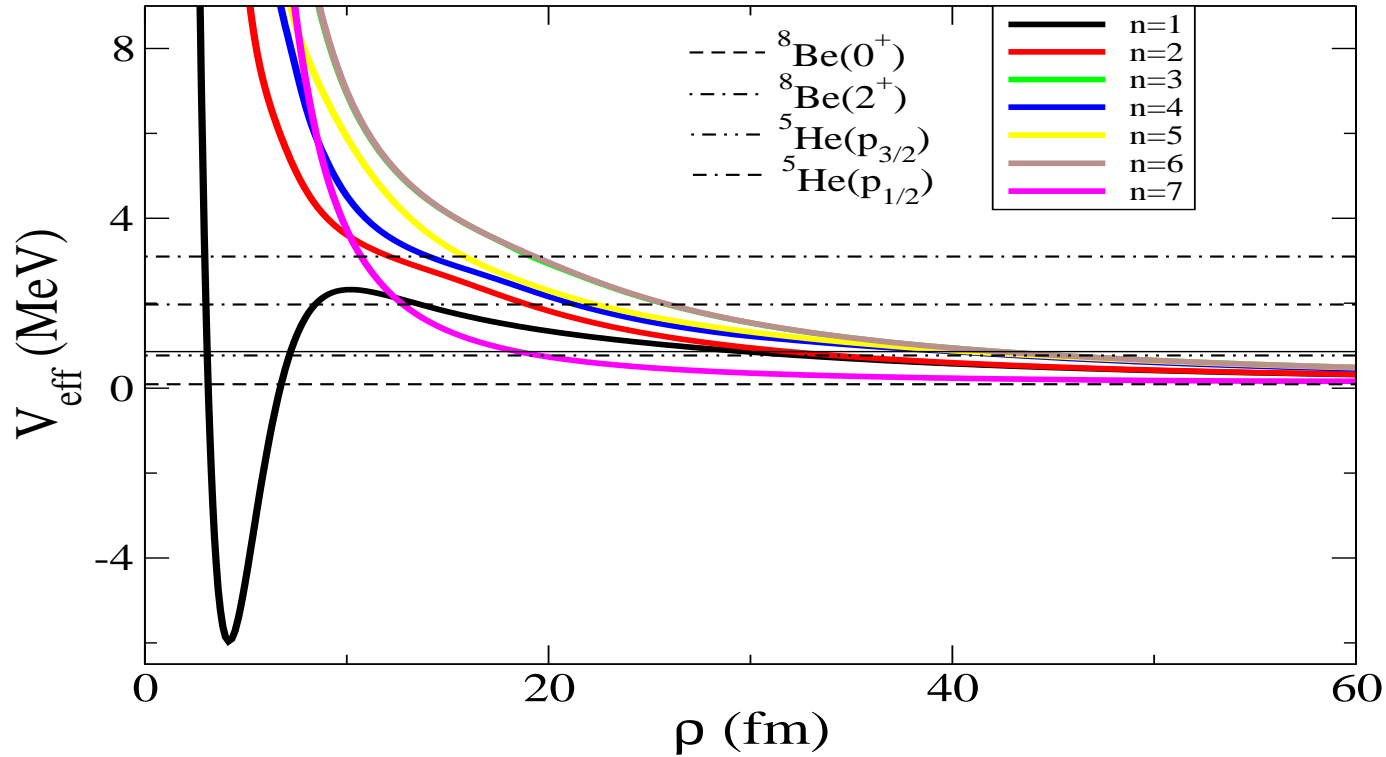


Figure 8: The real parts for  $\theta = 0.1$  of the lowest potentials, including the three-body potential, for the 0.856 MeV  ${}^9\text{Be}(5/2^-)$ -resonance (horizontal full line) as function of  $\rho$ .

## Systematics of low-energy $^9\text{Be}$ resonances

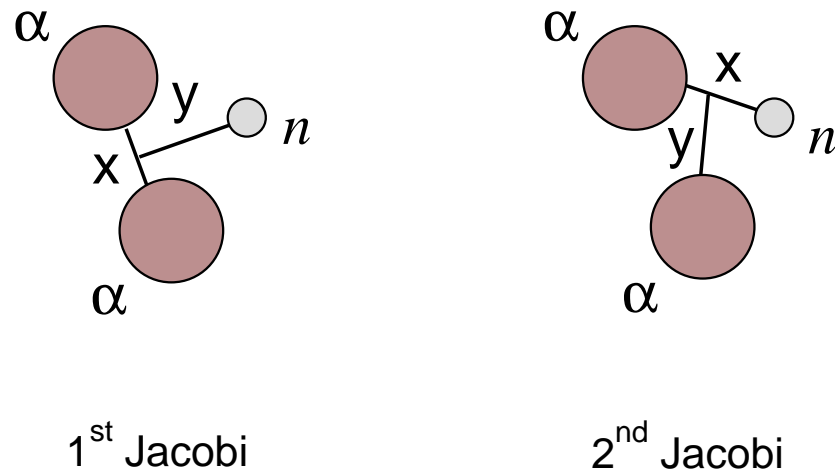


Figure 9: Scheme of the different Jacobi coordinates for  $^9\text{Be}$ . Each set of coordinates is complete and any function can be expressed in either of them.

One state, different basis,  ${}^8\text{Be}(2^+)$  or  ${}^5\text{He}(p_{3/2})$  and  ${}^5\text{He}(p_{1/2})$ .

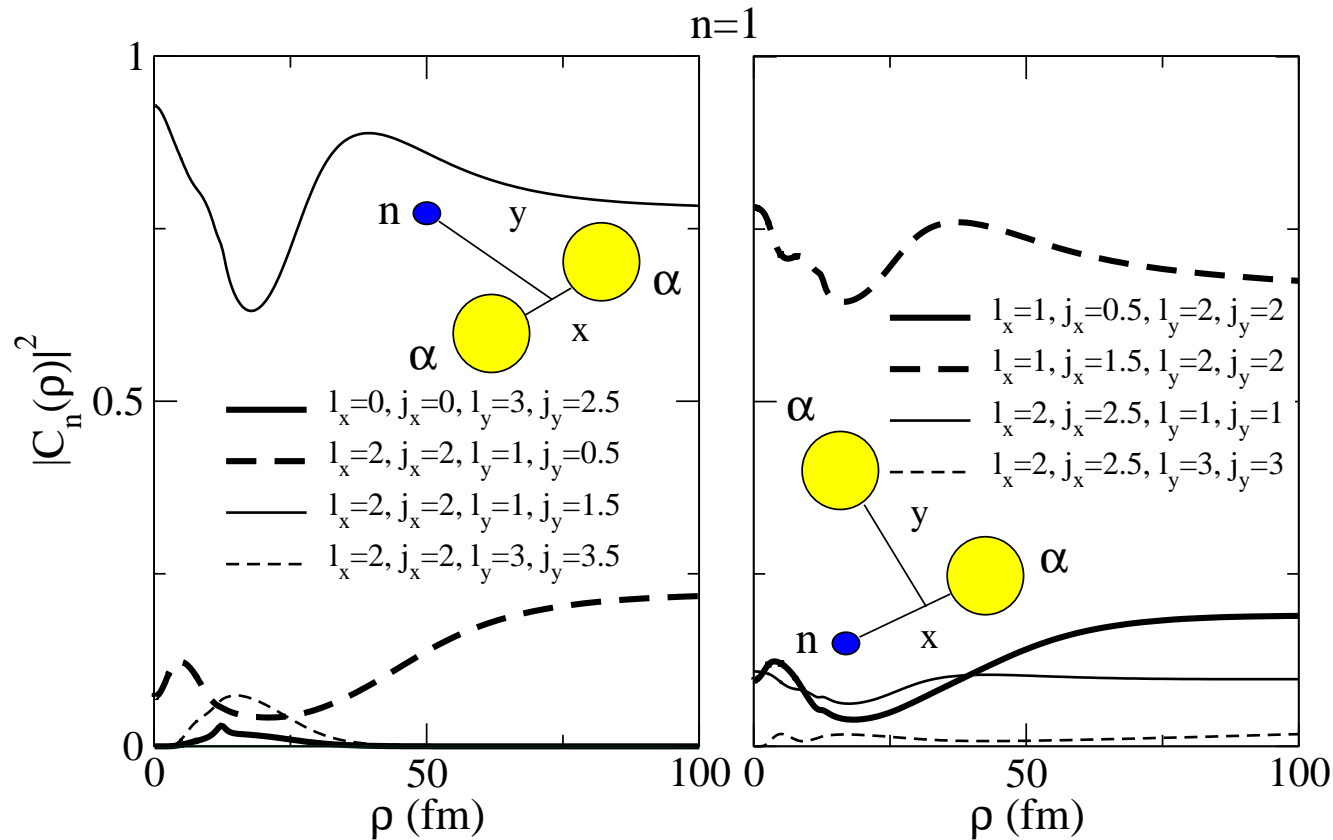


Figure 10: The partial wave decomposition in the two Jacobi coordinates of the dominating (96%) first adiabatic potential for the  ${}^9\text{Be}(5/2^-)$ -resonance.

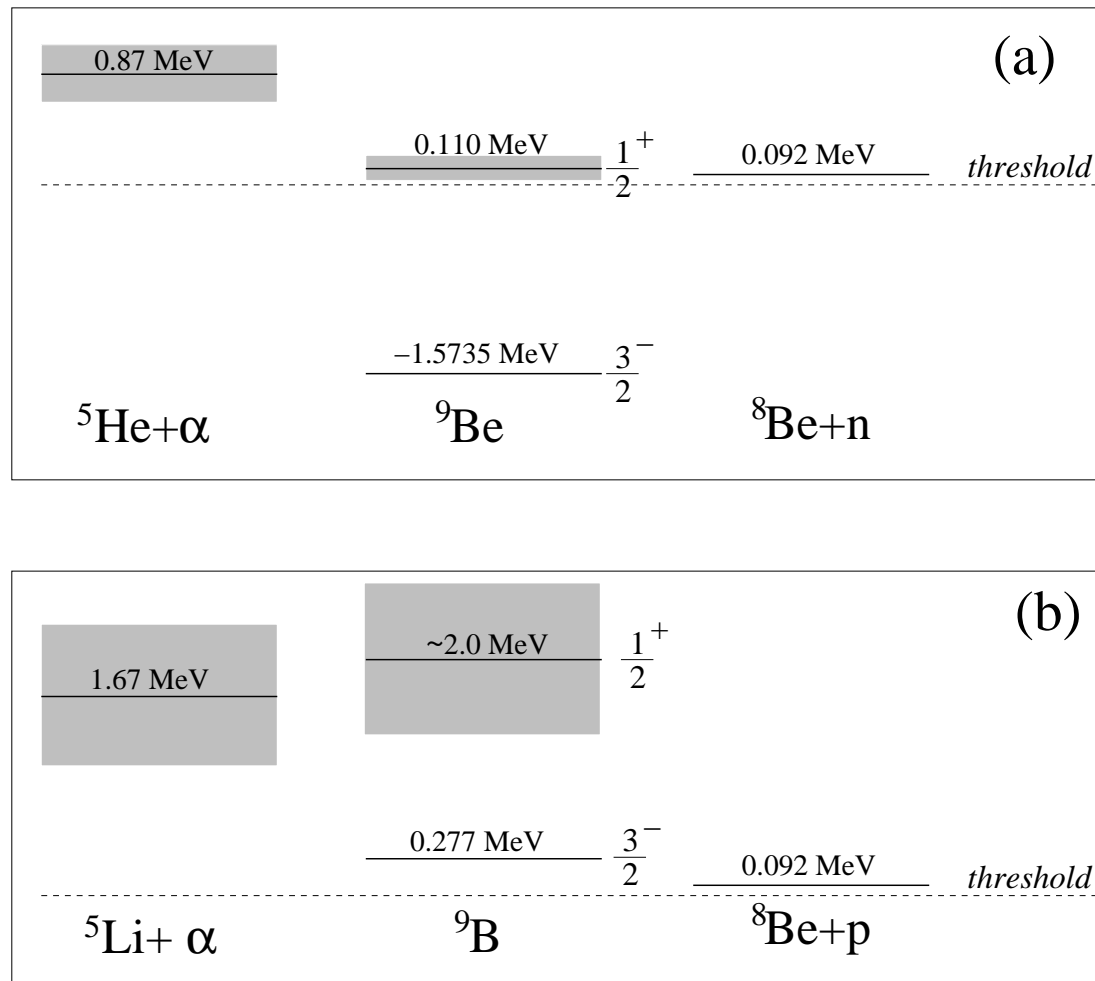


Figure 11: The two lowest energy levels for  ${}^9\text{Be}$  (a), and  ${}^9\text{B}$  (b), and the resonance energies of the corresponding two-body subsystems. For  ${}^9\text{B}$  the quoted  $1/2^+$  state corresponds to the estimation obtained in this work. The widths of the resonances are represented by the shadowed regions.

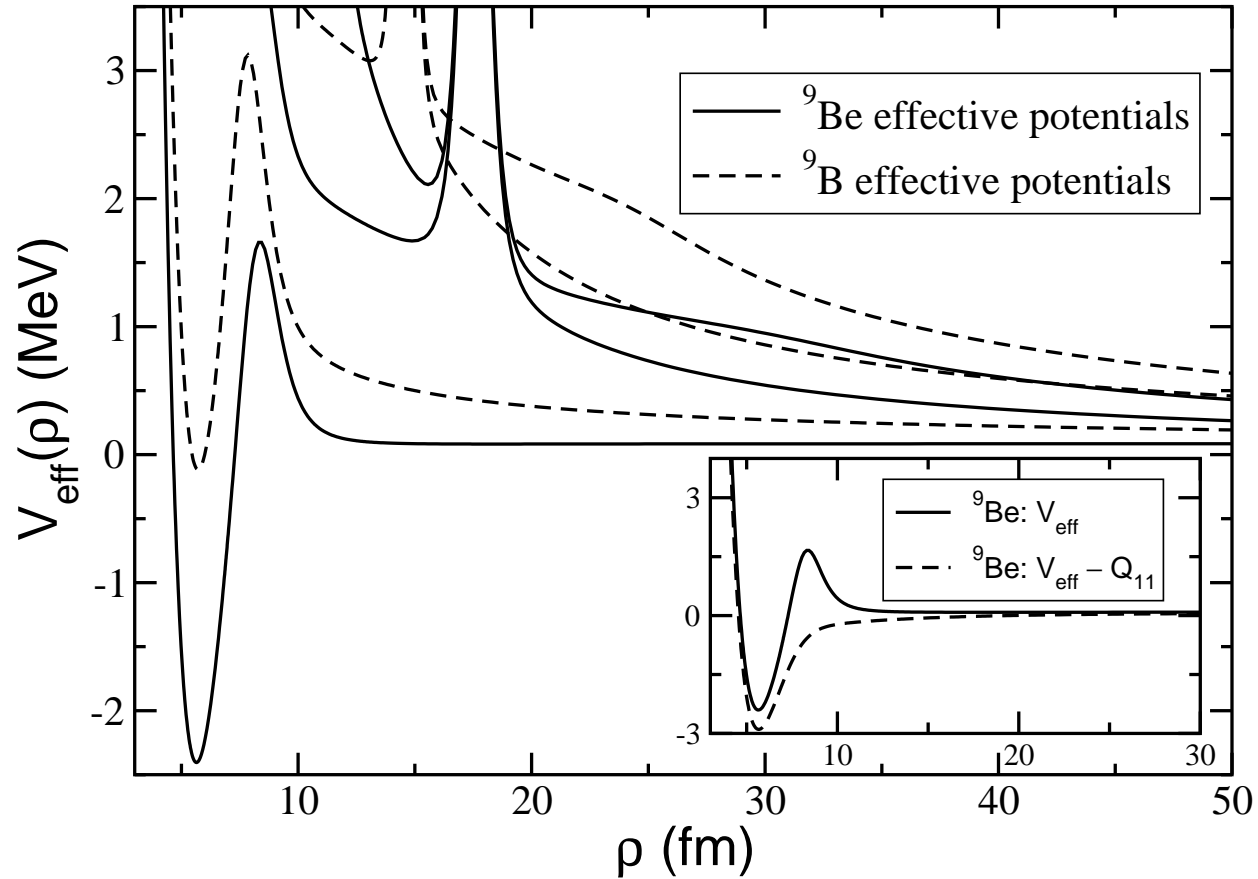


Figure 12: Lowest adiabatic potentials for  ${}^9\text{Be}$  and  ${}^9\text{B}$  as a function of the hyperradius. The inset shows the  ${}^9\text{Be}$  lowest potential with and without the rearrangement coupling term  $Q = \langle \phi | \frac{\partial^2}{\partial \rho^2} | \phi \rangle_{\Omega}$ .

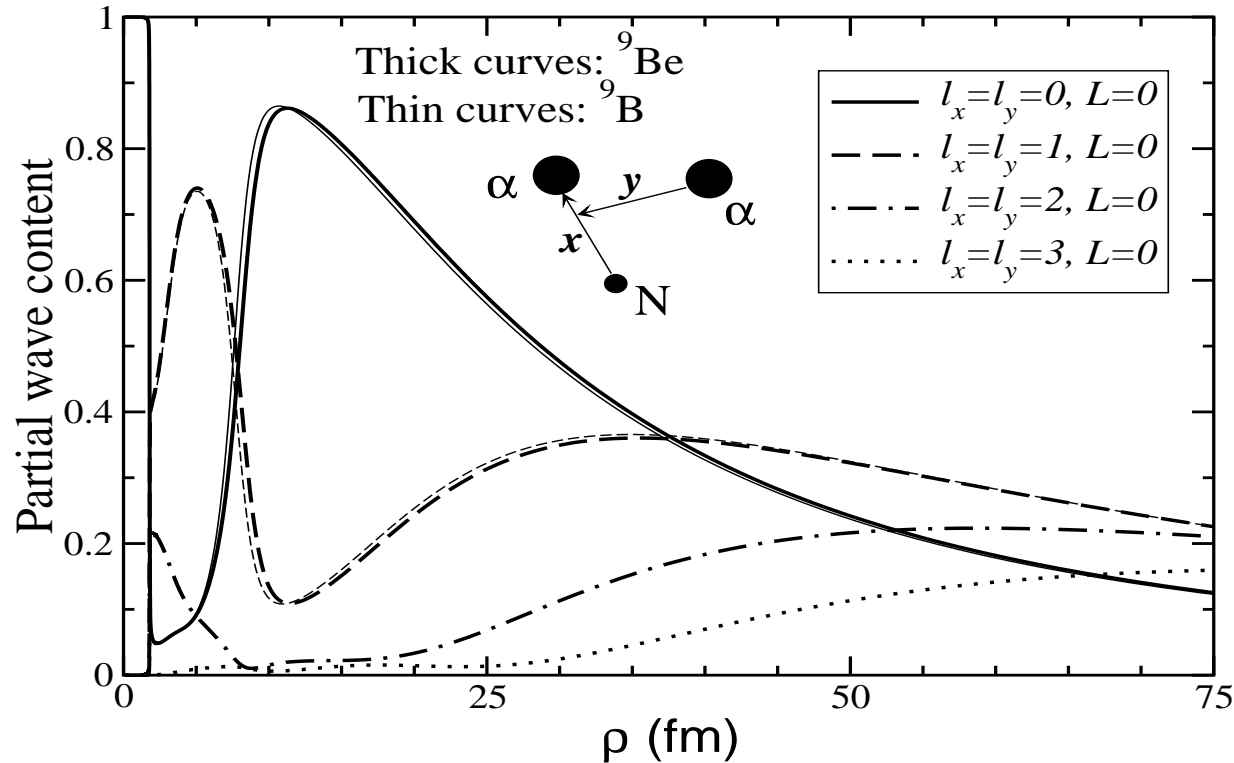


Figure 13: The partial wave decomposition of the lowest adiabatic angular wave function for  ${}^9\text{Be}$  (thick) and  ${}^9\text{B}$  (thin) as function of hyperradius  $\rho$ . The partial angular momenta  $l_x$  and  $l_y$  correspond to the coordinates indicated in the figure. For  $l_x = l_y = 2$  and  $l_x = l_y = 3$  the curves for  ${}^9\text{Be}$  and  ${}^9\text{B}$  can not be distinguished.

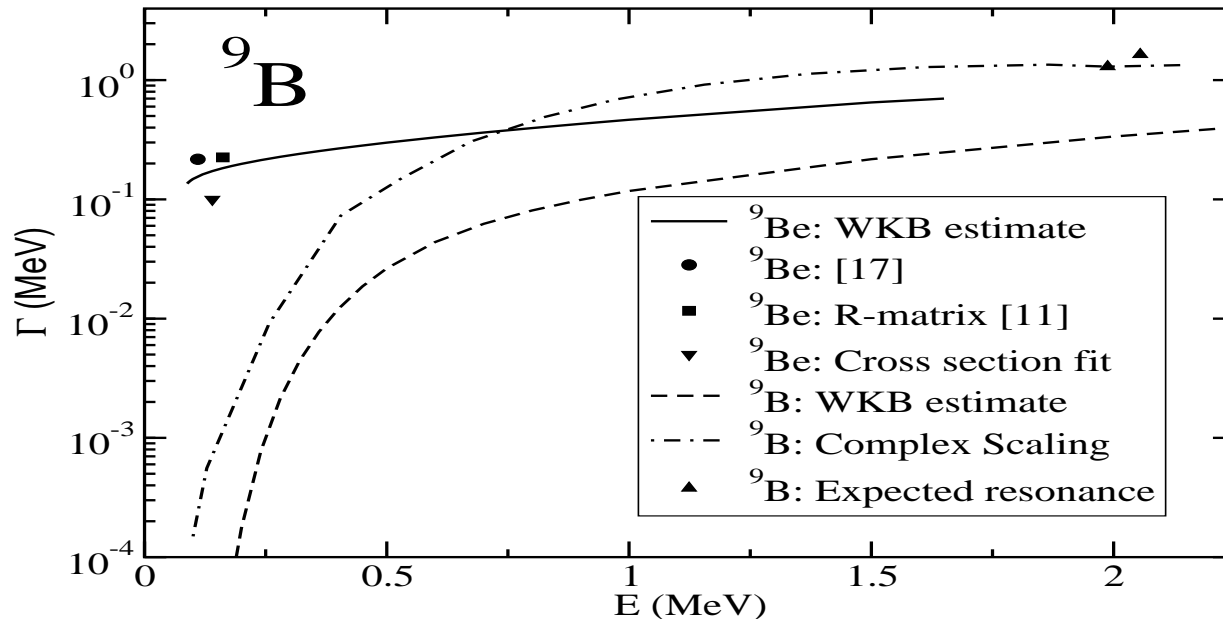


Figure 14: Width of the resonances for  ${}^9\text{Be}$  and  ${}^9\text{B}$  as function of the energy which is varied through the strength  $V_0$  of the three-body potential. The solid and dashed curves are the WKB results with a knocking rate corresponding to  $\Gamma_0 = 0.6$  MeV ( $\Gamma = \Gamma_0 e^{-2S}$ ) for both nuclei. The dot-dashed curve results from complex scaling for  ${}^9\text{B}$ . The square and the circle are from the R-matrix analysis in K. Sumiyoshi et al. NPA 709 (2002) 467 and the table in Tilley et al., NPA 745, 155 (2004). respectively. The down triangle is obtained by direct fit of the cross section in NPA 745, 155 (2002). The triangles at about 2 MeV are the first and second resonances of  ${}^9\text{B}$ .

## Dalitz plots

Theory and Experiments

Complete momentum distributions of all three particles

Detailed complete and accurate from measurements

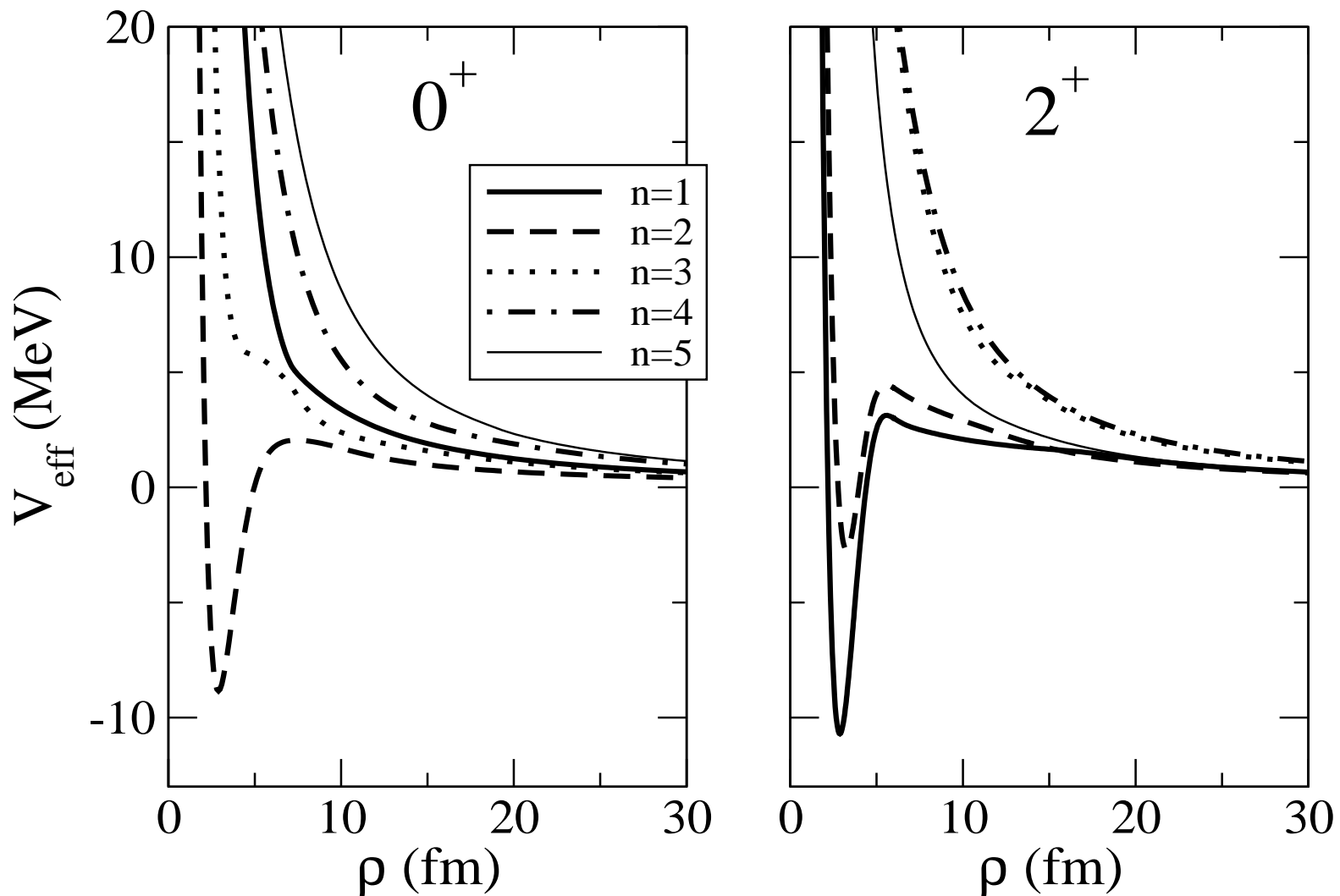


Figure 15: The real parts of the five lowest adiabatic effective potentials, including 3-body potential, as a function of the hyperradius for the  $0^+$  (left) and  $2^+$  (right) resonances of  ${}^6\text{Be}$ .

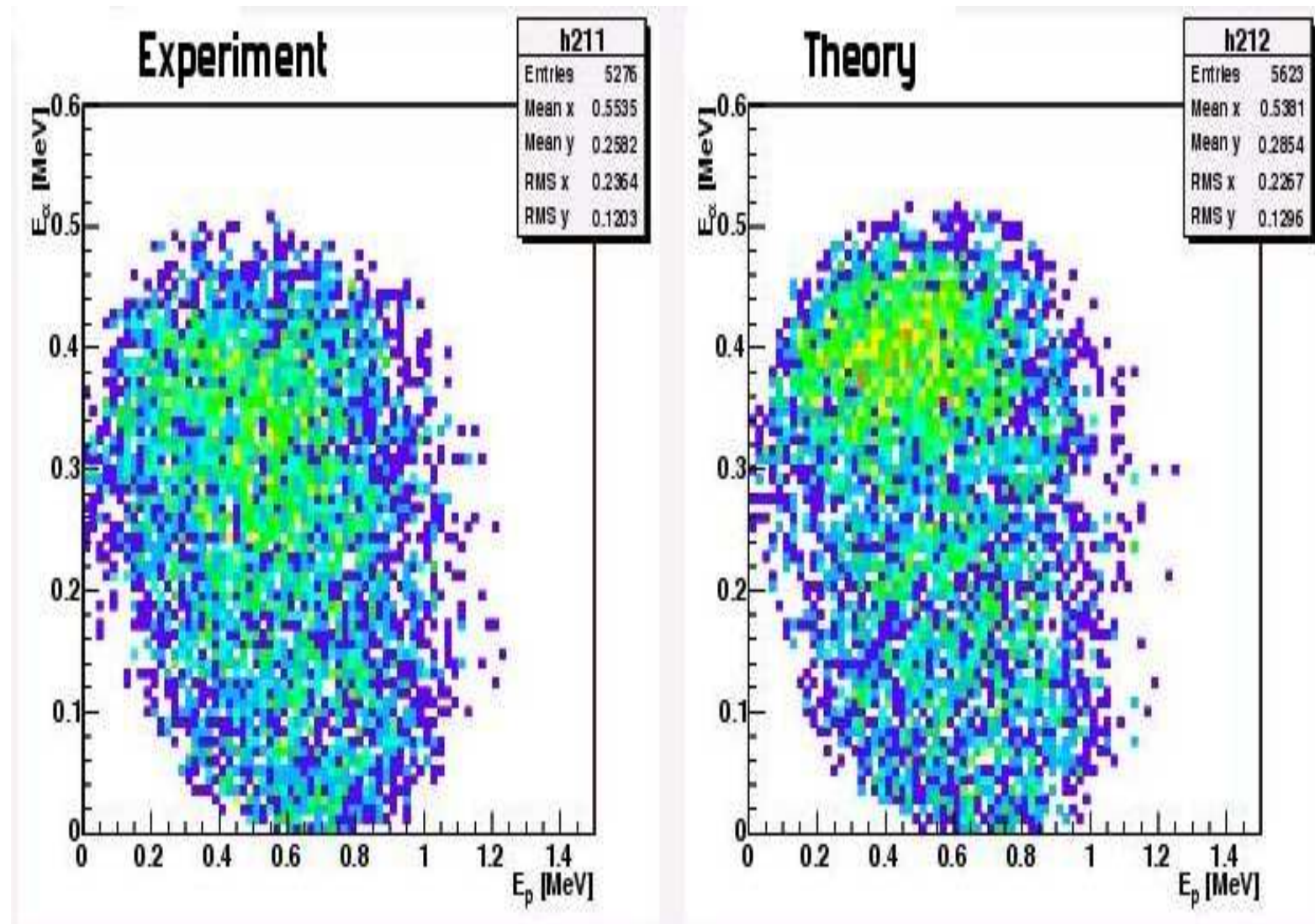


Figure 16: The computed Dalitz plots for the non-sequential part of the  ${}^6\text{Be}(0^+)$  decaying resonance, compared to the measured distribution from Papka et al., unpublished. Shown is the distribution of  $\alpha$ -energy versus proton-energy.

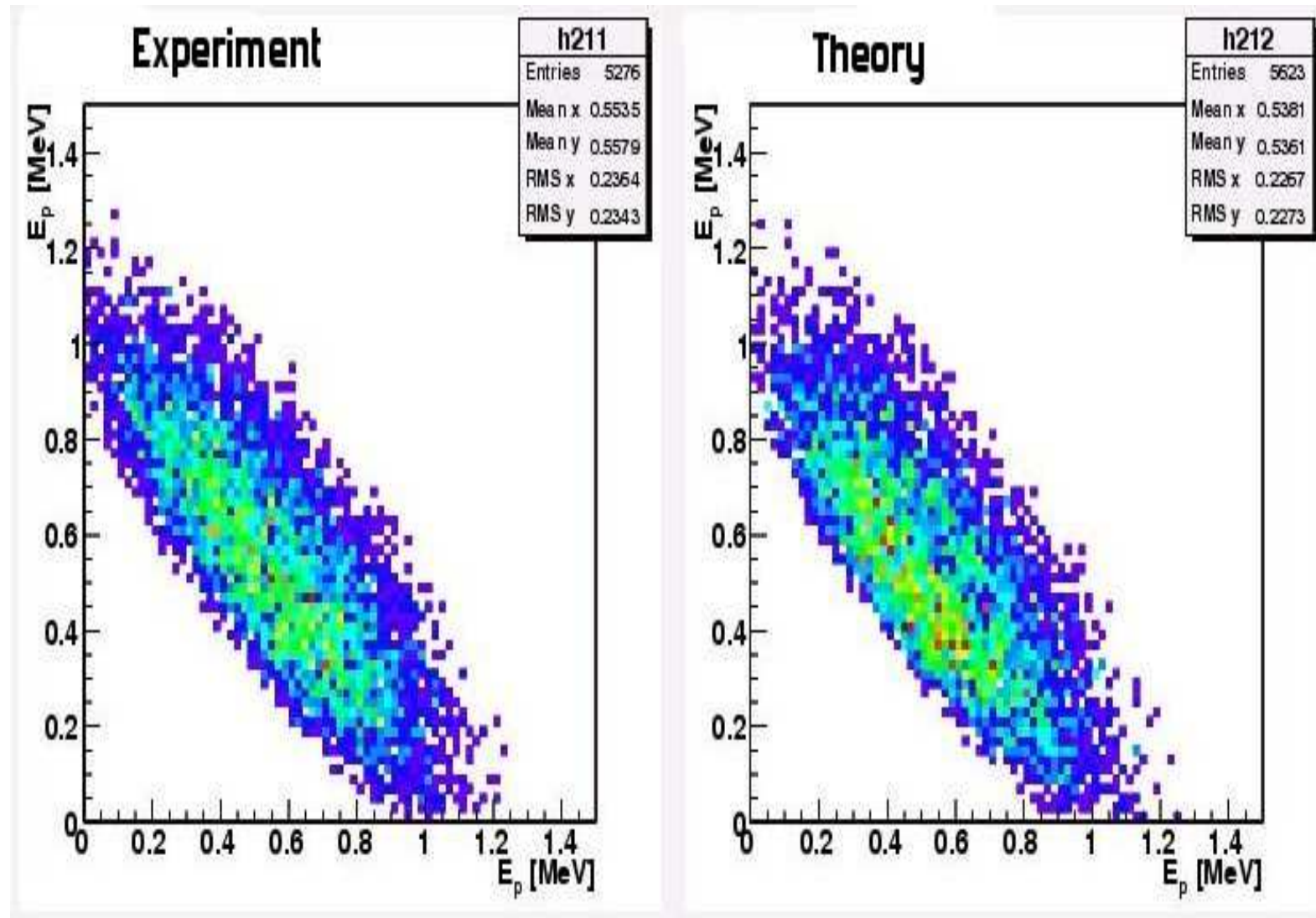


Figure 17: The computed Dalitz plots for the non-sequential part of the  ${}^6\text{Be}(0^+)$  decaying resonance, compared to the measured distribution from Papka et al., unpublished. Shown is the distribution of one proton-energy versus the other proton-energy.

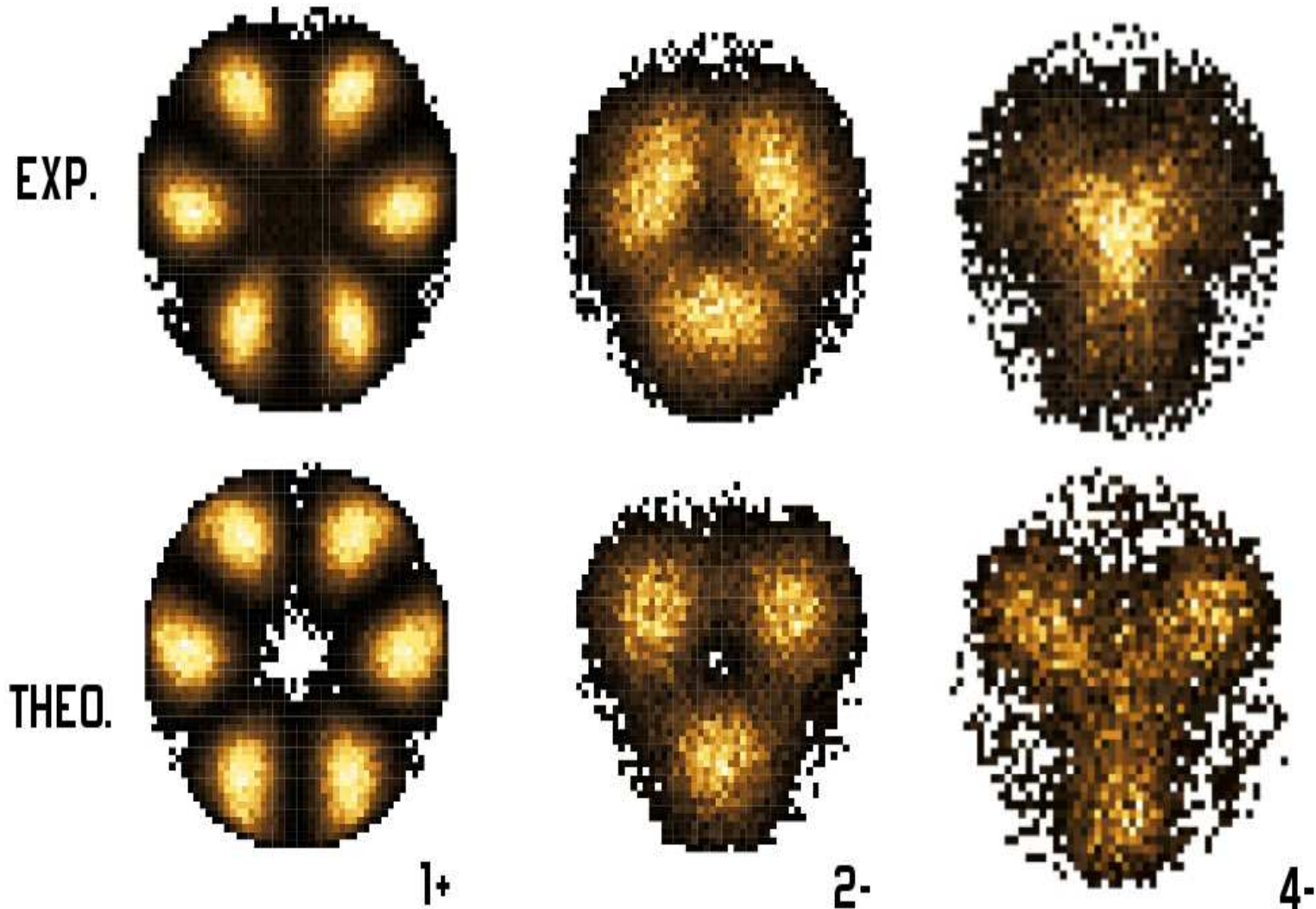


Figure 18: The computed Dalitz plots for  $^{12}\text{C}$  ( $1^+$ ,  $2^-$ ,  $4^-$ )-resonances, compared to similar measured distributions. Unpublished Kirsebom et al.

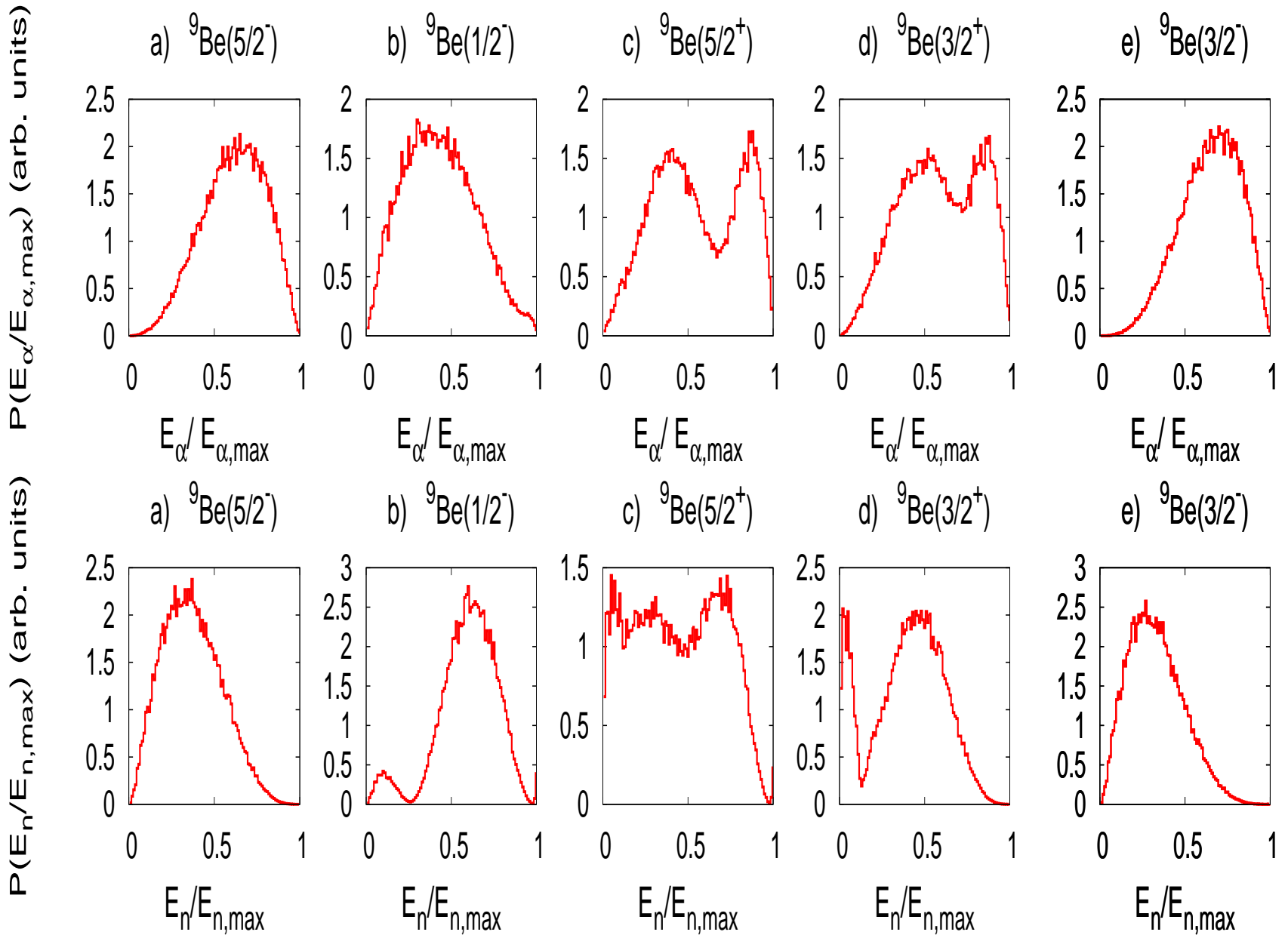


Figure 19: The  ${}^9\text{Be}$  resonances. Upper and lower parts are  $\alpha$ -particle and neutron energy distributions.

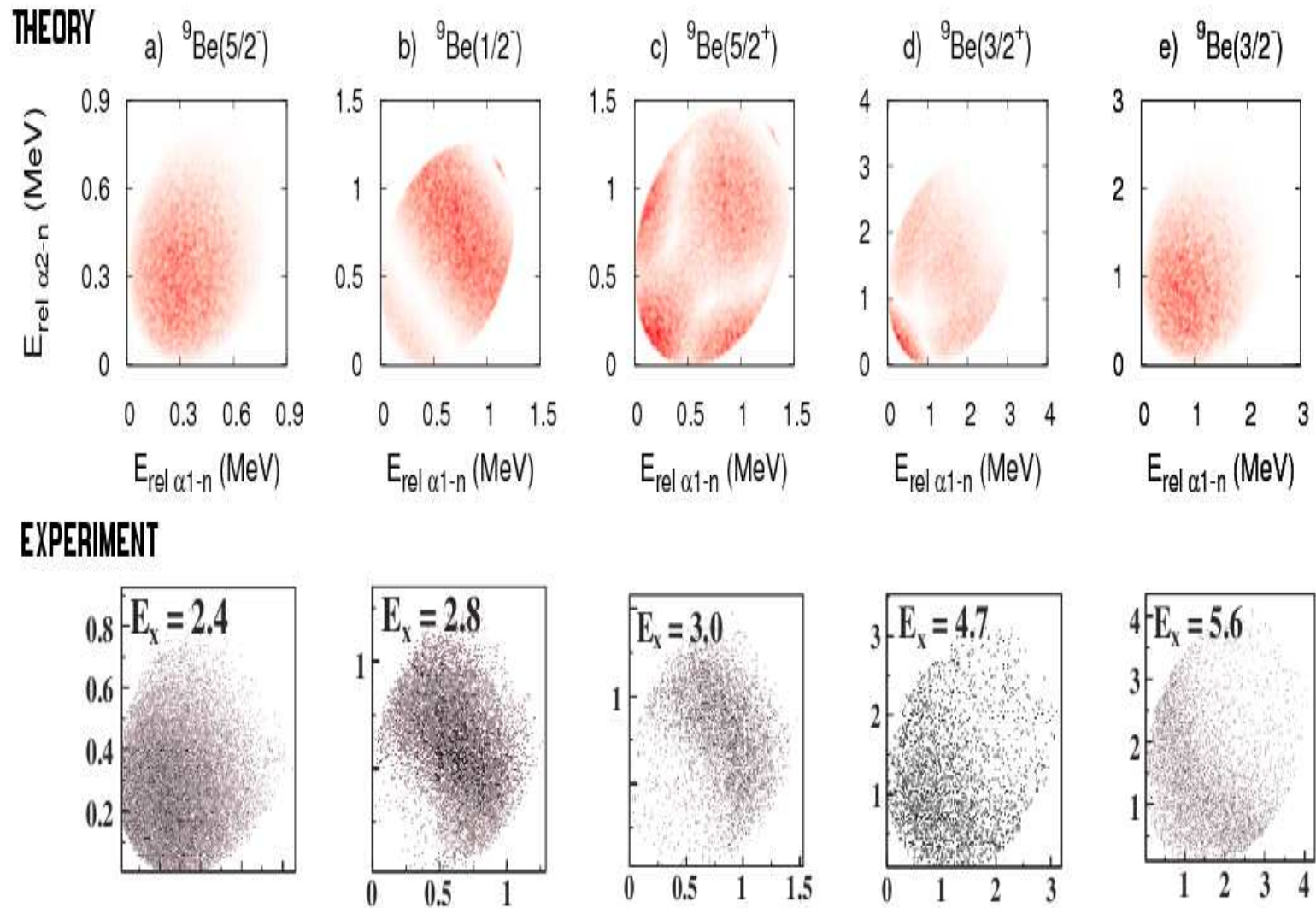


Figure 20: The computed Dalitz plots for various  ${}^9\text{Be}$  resonances, compared to similar measured distributions for the corresponding energy windows from Brown et al., PRC 76, 054605 (2007).

## Ultimate Limits: Our Existence?

Triple alpha rate is of prime importance

**Within high density or high temperature environments**

Rates of creation of:  ${}^6\text{He}$ ,  ${}^9\text{Be}$  and  ${}^{12}\text{C}$

Bridging the  $A = 5, 8$  gaps

## Astrophysical recombination processes

Three particles in the continuum combine into a bound state while emitting a photon. The rate is:

$$R_{abc}(E) = \frac{\hbar^3}{c^2} \frac{8\pi}{(\mu_x \mu_y)^{3/2}} \left( \frac{E_\gamma}{E} \right)^2 \frac{2g_A}{g_a g_b g_c} \sigma_\gamma(E_\gamma)$$

$$\sigma_\gamma^{(\lambda)}(E_\gamma) = \frac{(2\pi)^3 (\lambda+1)}{\lambda [(2\lambda+1)!!]^2} \left( \frac{E_\gamma}{\hbar c} \right)^{2\lambda-1} \frac{d\mathcal{B}}{dE}$$

Photo-dissociation cross section  $\sigma_\gamma^{(\lambda)}(E_\gamma)$  of multipolarity  $\lambda$ , and strength function  $\frac{d\mathcal{B}}{dE}$

## Density and temperature dependence

Average of rate over energy for given temperature gives:

$$P_{abc}(\rho, T) = n_a n_b n_c \frac{\hbar^3}{c^2} \frac{8\pi}{(\mu_x \mu_y)^{3/2}} \frac{g_A}{g_a g_b g_c} e^{-\frac{B}{k_B T}} \\ \times \frac{1}{(k_B T)^3} \int_{|B|}^{\infty} E_\gamma^2 \sigma_\gamma(E_\gamma) e^{-\frac{E_\gamma}{k_B T}} dE_\gamma$$

$n_i = \rho N_A X_i / A_i$  is density fraction of total  $\rho$

$$X_i = N_i M_i / (N_a M_a + N_b M_b + N_c M_c),$$

$M_i$  and  $N_i$  are mass and number of particle species  $i$

$Y_i = N_i / (N_a + N_b + N_c)$  is relative abundance

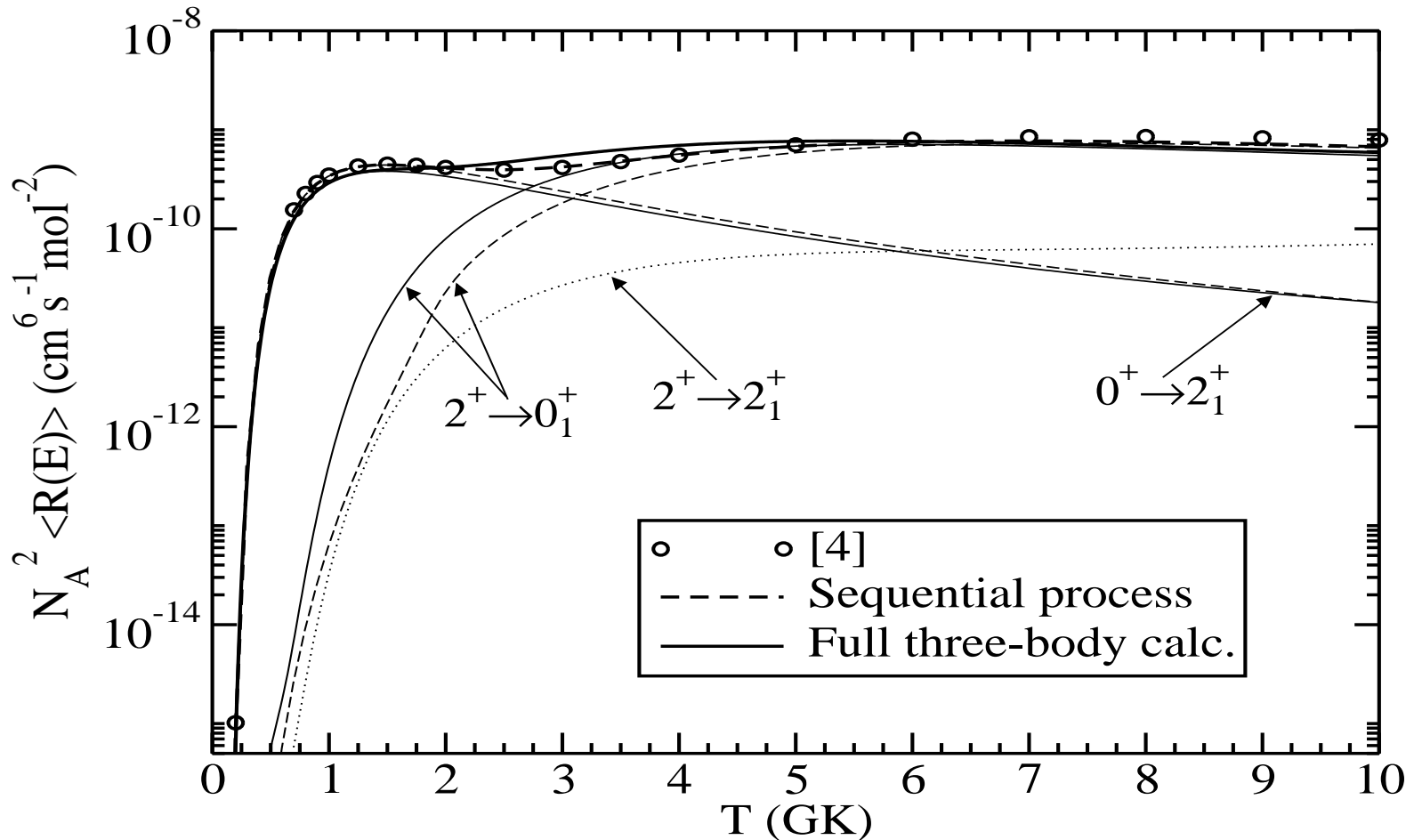
Triple  $\alpha$ -process

Figure 21: Reaction rate for the triple  $\alpha$  process with the full three-body calculation (thick solid line) and the sequential approach (thick dashed line) as described in the text. The corresponding contributions from the  $0^+ \rightarrow 2_1^+$  and  $2^+ \rightarrow 0_1^+$  transitions are given by the thin curves. The dotted line is the contribution from the  $2^+ \rightarrow 2_1^+$  in the full three-body calculation. The open circles correspond the rate given in Angulo et al.

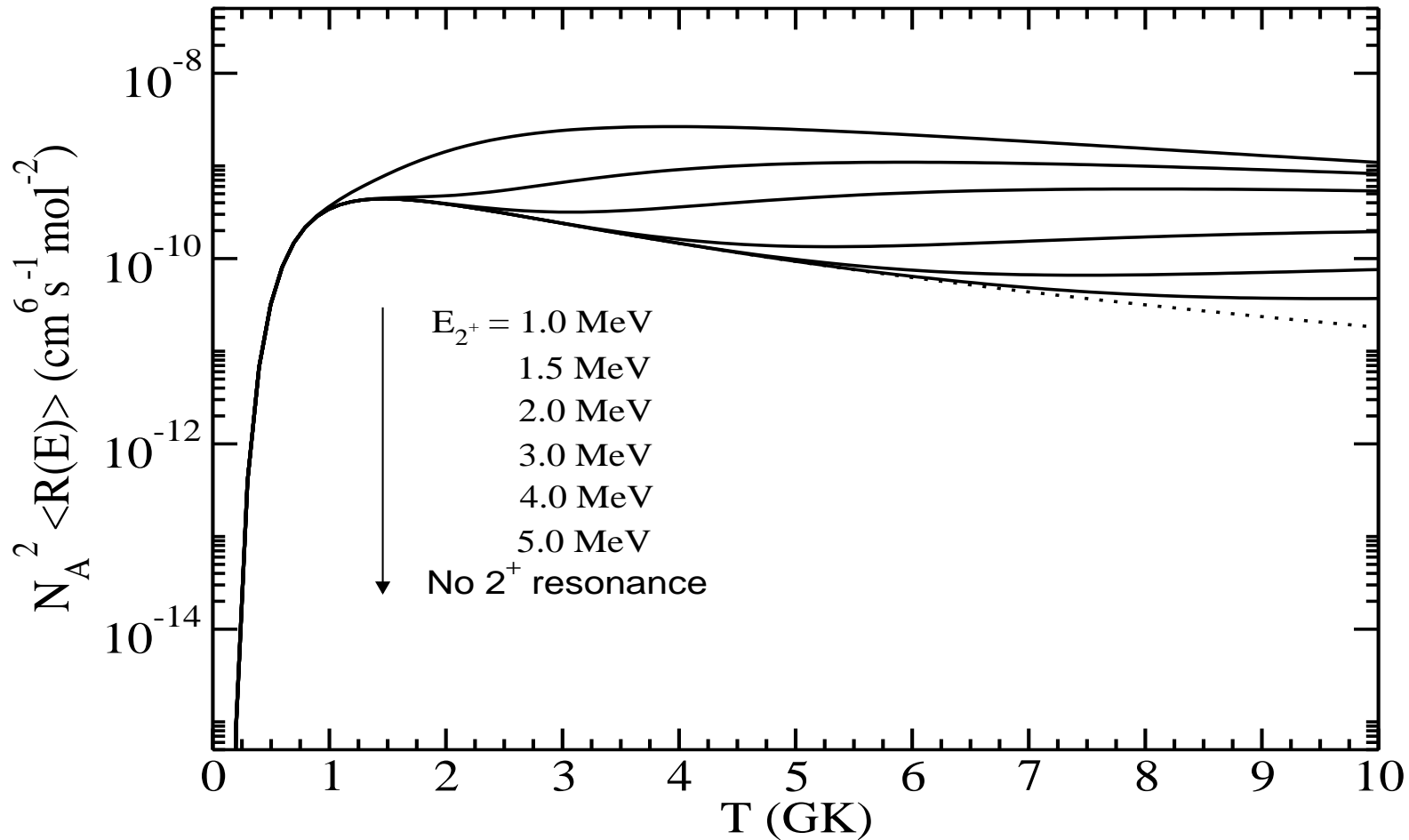


Figure 22: Reaction rate in the sequential case for different energies of the lowest  $2^+$  resonance in  $^{12}\text{C}$ . The energy increases from the upper curve to the lower from 1 MeV up to 5 MeV. The dotted curve is the calculation where the contribution from the  $2^+ \rightarrow 0_1^+$  transition has been completely removed.

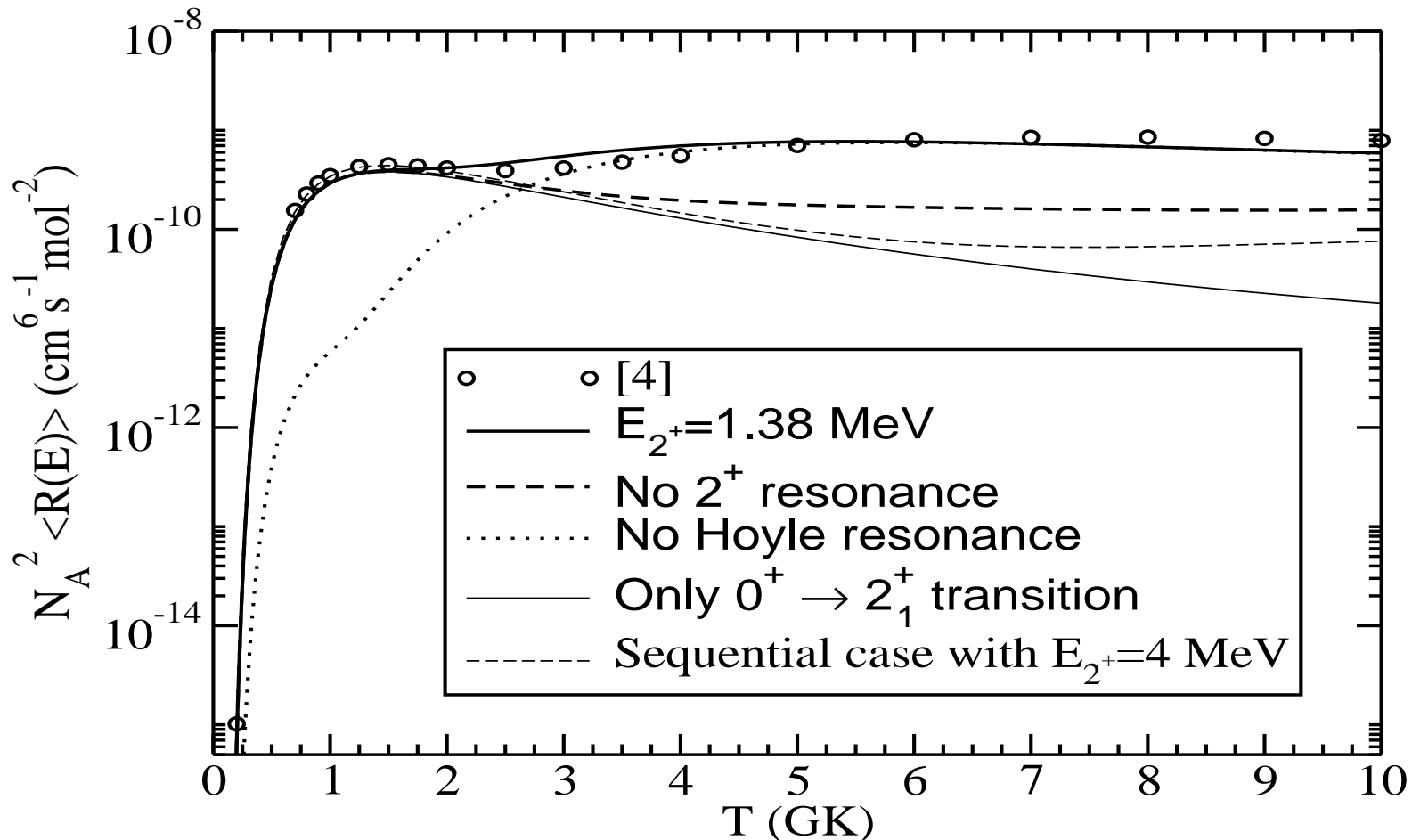


Figure 23: Reaction rate after the full three-body calculation when the  $2^+$  resonance is placed at 1.38 MeV (thick solid line), when the resonance is removed from the calculation (thick dashed line), when the full contribution from the  $2^+ \rightarrow 0_1^+$  transition is excluded (thin solid line), and when the Hoyle resonance is removed (dotted line). The thin solid curve is the calculation in the sequential case when the energy of the  $2^+$  resonance is 4.0 MeV. The open circles are the rate from Angulo et al. 1999.

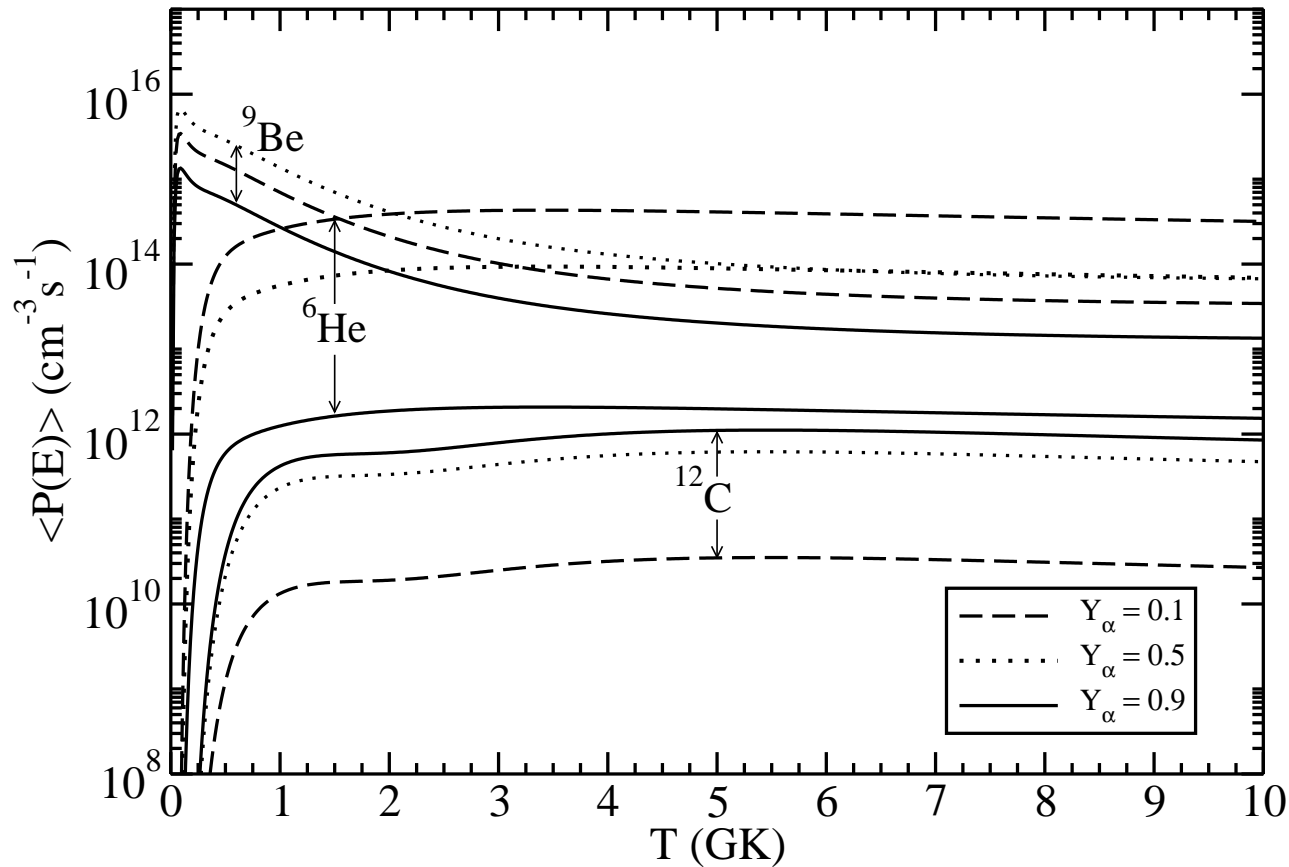


Figure 24: The numbers of produced  ${}^6\text{He}$ ,  ${}^9\text{Be}$  and  ${}^{12}\text{C}$  per unit time and volume as functions of temperature for  $Y_\alpha = 0.1$  (dashed),  $0.5$  (dotted), and  $0.9$  (solid) and a density  $\rho = 1 \text{ g/cm}^3$ .

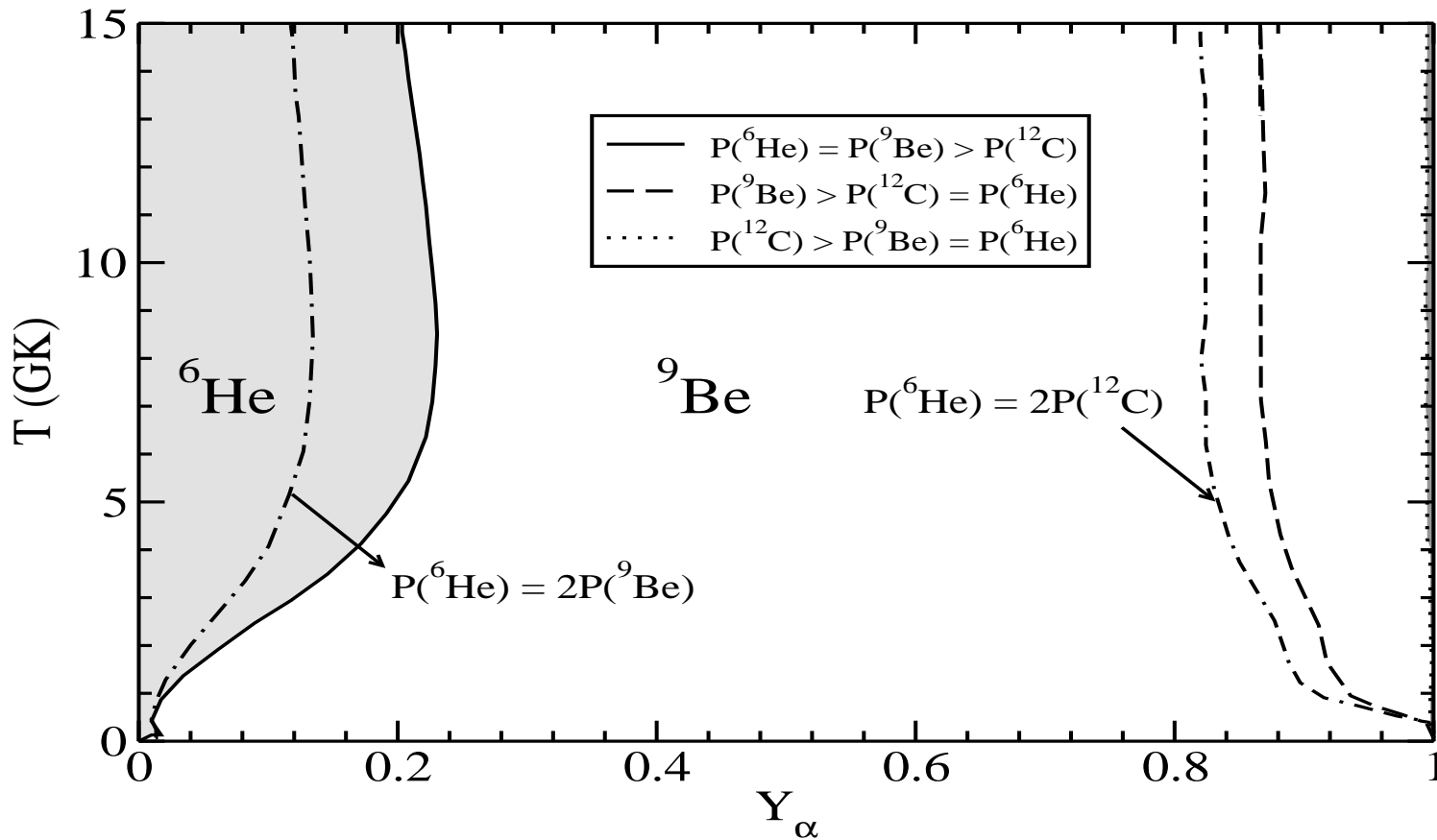


Figure 25: The phase diagram for producing  ${}^6\text{He}$ ,  ${}^9\text{Be}$  and  ${}^{12}\text{C}$  in the  $Y_\alpha$ -temperature parameter space. The curves correspond to a constant ratio of production rates of two nuclei.

## Four-body recombination

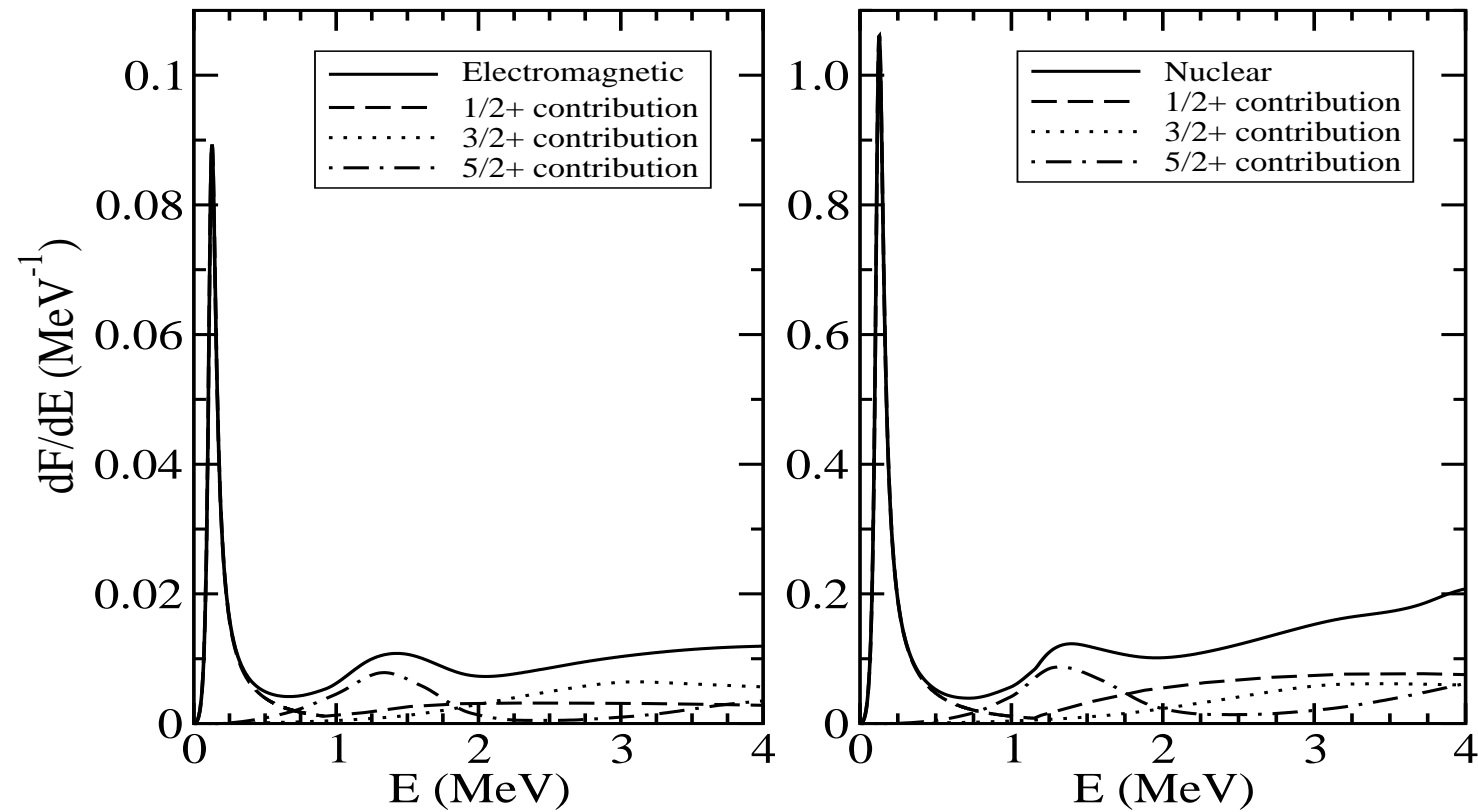


Figure 26: The strength functions for  ${}^9\text{Be}$  recombination from electromagnetic and nuclear processes.

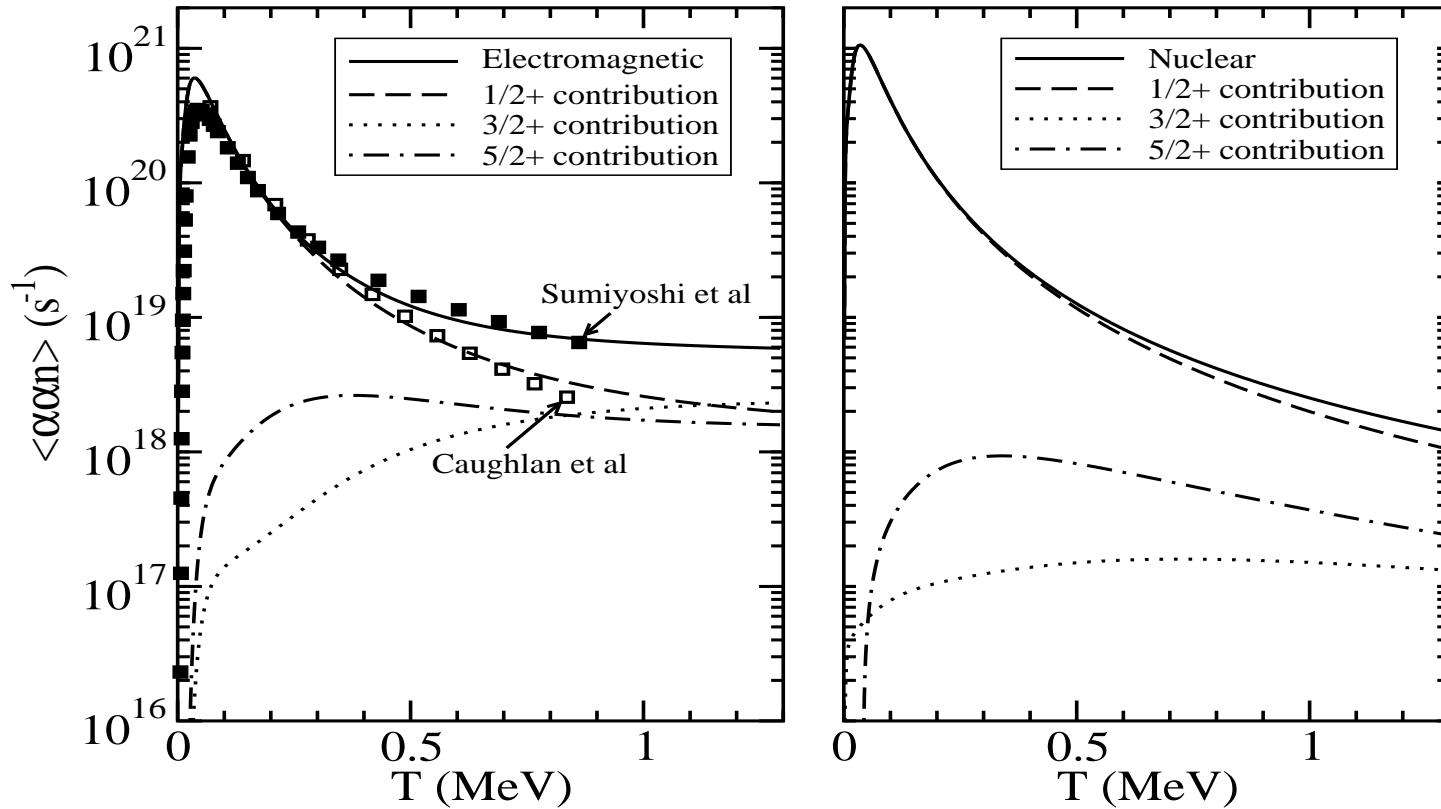


Figure 27: The temperature averaged rates for  ${}^9\text{Be}$  recombination from electromagnetic and nuclear processes. The nuclear rate is calculated for the neutron density of  $10^{30} \text{ cm}^{-3}$

## Summary of issues

Limits to existence of light nuclei:

Binding energies approaching zero, scaling properties

Structure under sea level, reefs outside the driplines

Resonances and continuum states with a lifetime,  ${}^9\text{Be}(1/2^+)$

Triple alpha rates  ${}^{12}\text{C}(2^+)$  and other three-body rates

Dynamical evolution, sequential and/or direct, Dalitz plots,  ${}^9\text{Be}$ ,  ${}^6\text{Be}$

Rates in high density or high temperature environments

Four-body rates as alternative astrophysical process

## Numerical and method requirements

Accuracy

Basis size, i.e. numbers of:

partial waves

adiabatic potentials

hyperspherical polynomials

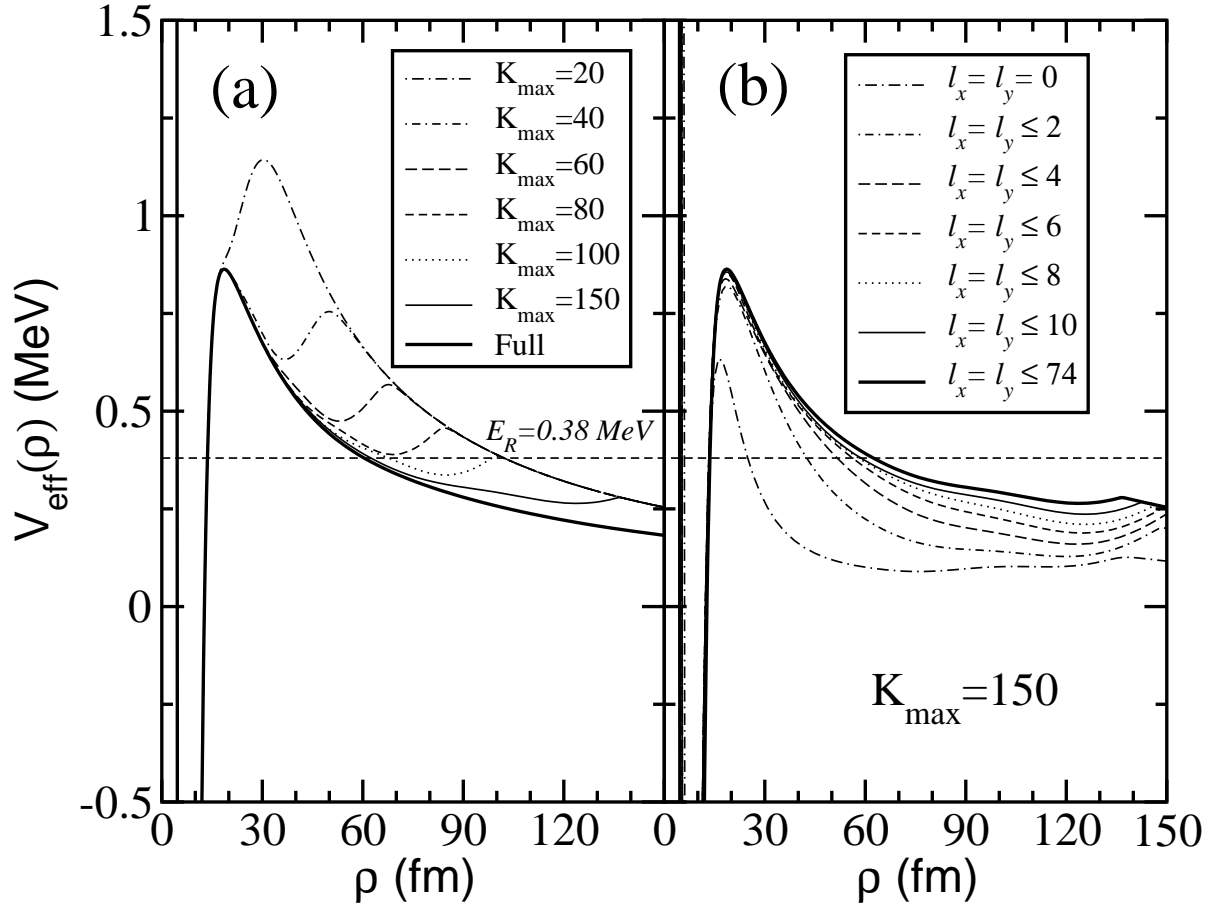


Figure 28: The dominating effective adiabatic potential for the lowest  $0^+$  resonance in  $^{12}\text{C}$  ( $\alpha+\alpha+\alpha$ ) for (a) different values of  $K_{\text{max}}$  and (b) different values of partial waves in the expansion in terms of HH. The dashed straight line indicates the energy of the resonance. In (a) all the possible values of  $l_x$  and  $l_y$  consistent with  $K_{\text{max}}$  have been included. The curve called “full” includes  $l_x = l_y$  up to 12 only and  $K_{\text{max}}=150$ , but with  $K_{\text{max}}$  increased up to 500 for some of the components. In (b)  $K_{\text{max}} = 150$ .

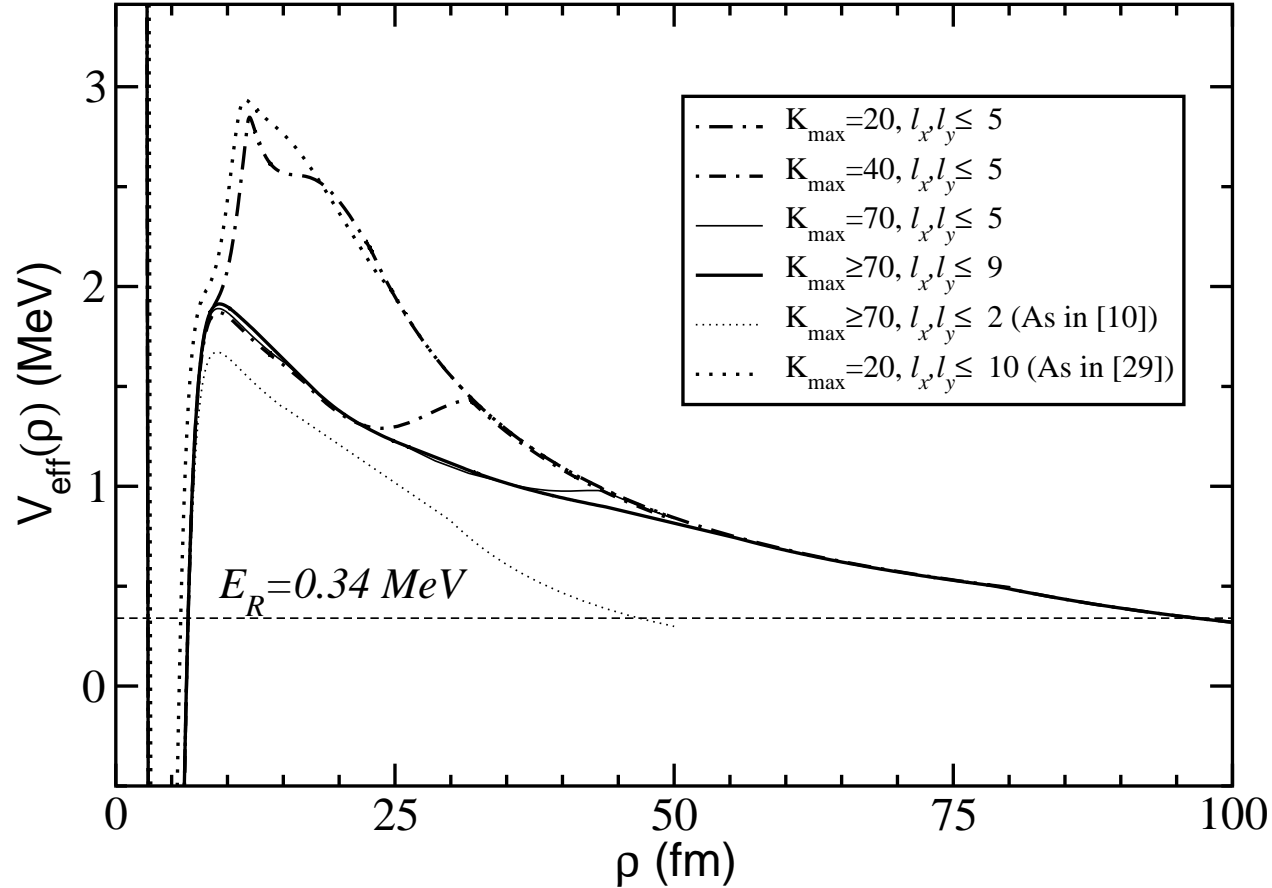


Figure 29: Lowest adiabatic effective potential for the  $3/2^-$  resonance in  $^{17}\text{Ne}$ . Except for the last curve (thick-dot), the  $p$ - $^{15}\text{O}$  interaction is the one described in NPA 733, 85 (2004). The different curves correspond to calculations with different values of  $K_{\text{max}}$  and relative two-body angular momenta. The thin-dotted curve corresponds to the calculation presented in NPA 733, 85 (2004). In the last (thick-dotted) curve, the  $p$ - $^{15}\text{O}$  potential and  $K_{\text{max}}$  value of NPA 713, 372 (2003) have been used. The dashed straight line indicates the resonance energy of 0.34 MeV.

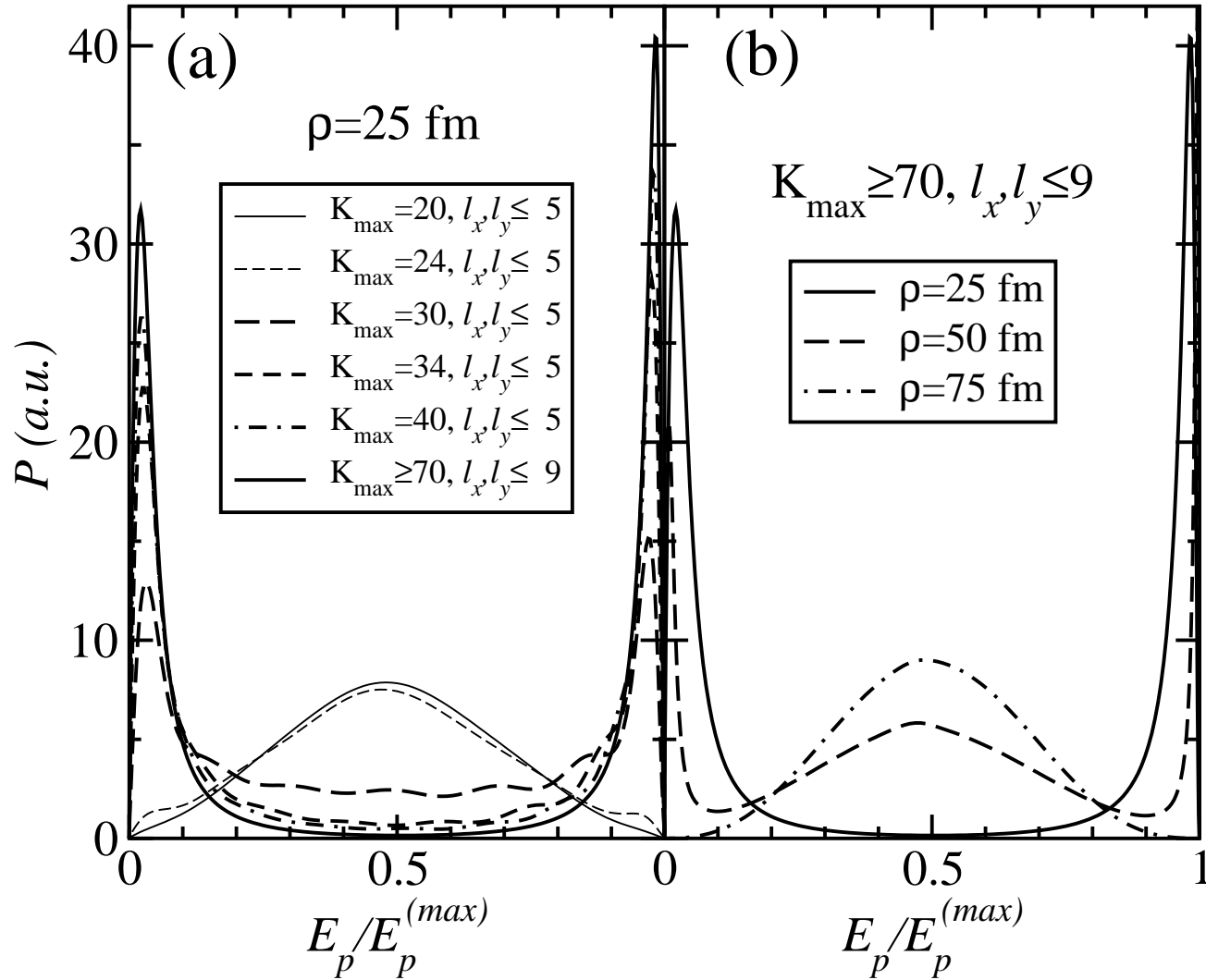


Figure 30: Proton energy distributions for the  $3/2^-$  resonance in  $^{17}\text{Ne}$  where the maximum allowed emission energy is used as unit. The left part is for  $\rho=25$  fm for different values of  $K_{max}$ . The right part is for a very large basis for increasing hyperradii. Only the lowest adiabatic effective potential is used.

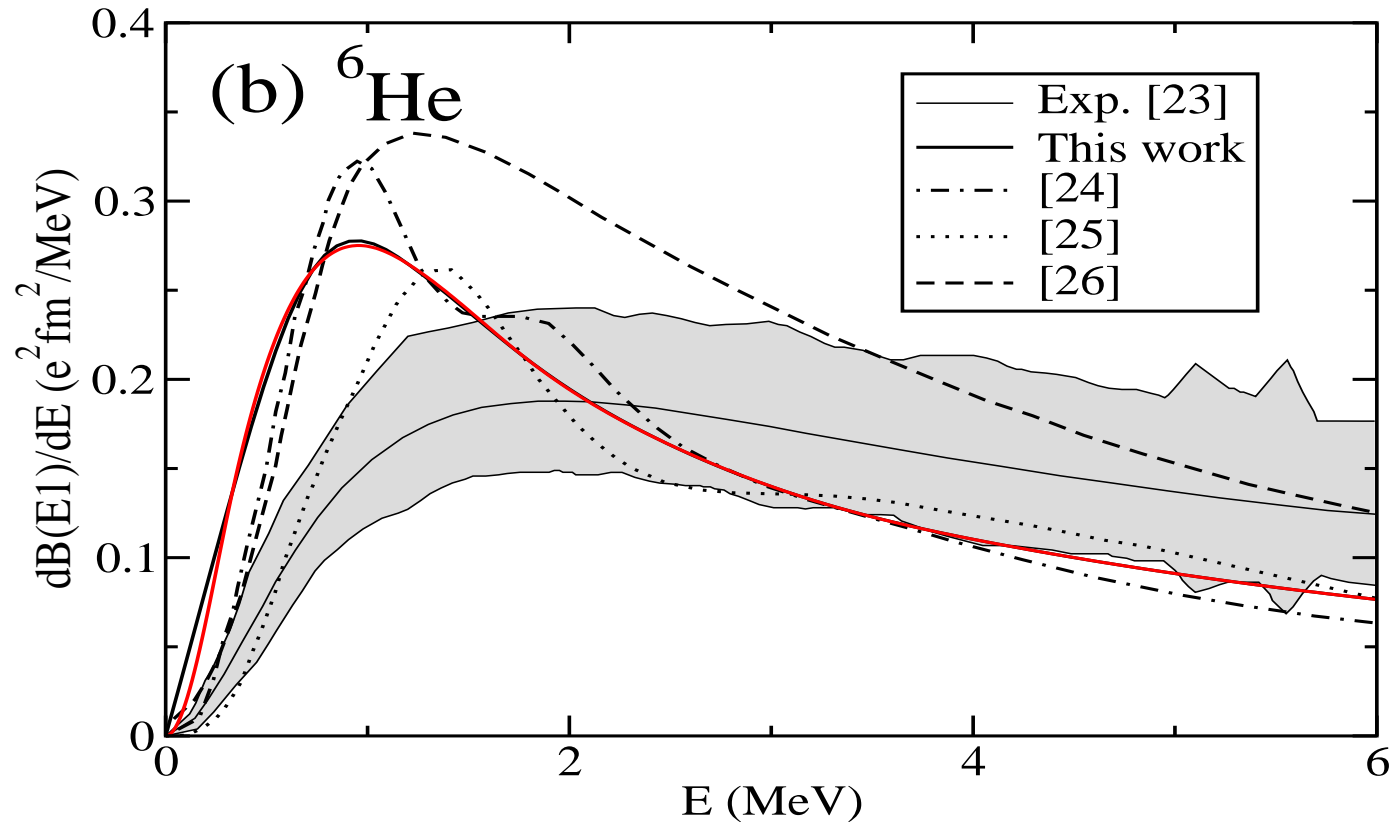


Figure 31: Comparison between different computed dipole strength for  ${}^6\text{He}$  and experimental data, the shaded area, see [23] T.Aumann et al., PRC59, 1252 (1999), [24] A.Cobis et al., PRL 79, 2411 (1997), [25] T. Myo et al., PRC 63, 054313 (2001), [26] B.V.Danilin et al., NPA 632, 383 (1998).

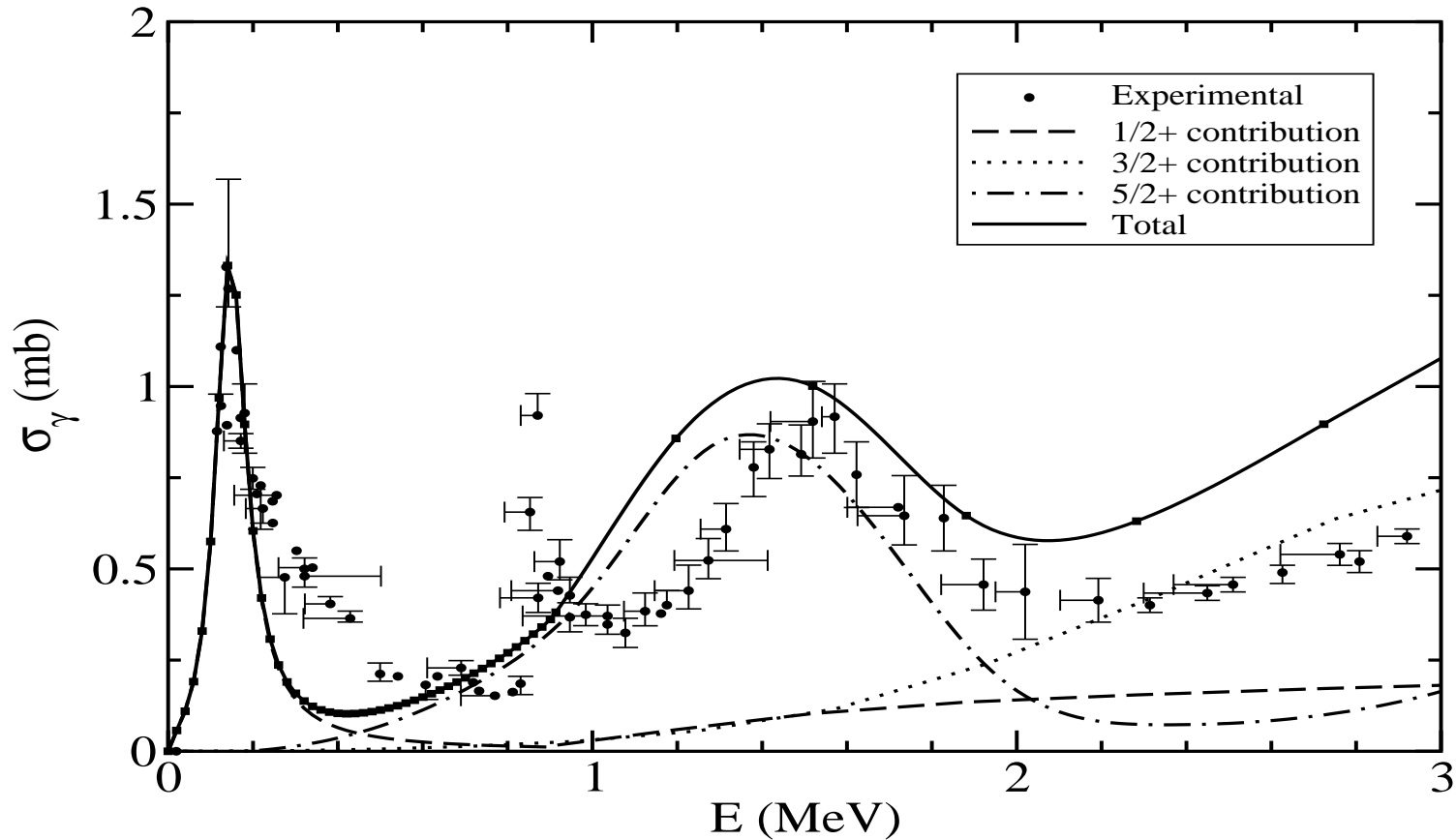


Figure 32: Photodissociation cross section for  ${}^9\text{Be}$ . The total computed cross section is given by the solid line. The contributions from transitions to the  $1/2^+$ ,  $3/2^+$ , and  $5/2^+$  continuum three-body states are given by the dashed, dotted, and dot-dashed curves, respectively. The experimental data are from K. Sumiyoshi et al., NPA 709, 467 (2002).

## References

- [1] A.S. Jensen and K. Riisager, Stable nuclear structure beyond the drip-line?, *Phys. Lett.* **B264**, 238 (1991).
- [2] A.S. Jensen and K. Riisager, Stable nuclear structure along the drip-line?, *Nucl. Phys.* **A537**, 45 (1992).
- [3] D.V. Fedorov and A.S. Jensen, *Phys.Lett.* **B389**, 631 (1996).
- [4] A. Cobis, D.V Fedorov, and A.S. Jensen, *Phys. Rev. Lett.* **79**, 2411 (1997).
- [5] D.V. Fedorov, A. Cobis and A.S. Jensen, *Phys. Rev.* **C59**, 554 (1999).
- [6] E. Nielsen, D.V. Fedorov, A.S. Jensen, and E. Garrido, *Phys. Rep.* **347**, 373 (2001).
- [7] E. Garrido, D.V. Fedorov and A.S. Jensen, *Nucl. Phys.* **A 708**, 277 (2002).
- [8] E. Garrido, D.V. Fedorov, and A.S. Jensen, *Phys. Rev. C* **68**, 014002 (2003).
- [9] A.S. Jensen, K. Riisager, D.V. Fedorov and E. Garrido, *Europhysics Lett.* **61**, 320-326 (2003).
- [10] D.V. Fedorov, E. Garrido, and A.S. Jensen, *Few-body systems*, **33**, 153-171 (2003).
- [11] A.S. Jensen, K. Riisager, D.V. Fedorov and E. Garrido, *Rev. Mod. Phys.* **76** (2004) 215-261.
- [12] E. Garrido, D.V. Fedorov and A.S. Jensen, *Phys.Rev.* **C 69**, 024002 (2004).
- [13] E. Garrido, D.V. Fedorov and A.S. Jensen, *Nucl. Phys.* **A 733**, 85-109 (2004).

- [14] A.S. Jensen, K. Riisager, D.V. Fedorov and E. Garrido, *Rev. Mod. Phys.* **76** (2004) 215-261.
- [15] E. Garrido, D.V. Fedorov, and A.S. Jensen, *Nucl. Phys. A* **733**, 85 (2004).
- [16] D. V. Fedorov, H. O. U. Fynbo, E. Garrido, and A.S. Jensen, *Few-Body Syst.* **34**, 33 (2004).
- [17] D.V. Fedorov, H.O.U. Fynbo, E.Garrido and A.S. Jensen, *Few-body systems*, **34**, 33-37 (2004).
- [18] E. Garrido, D.V. Fedorov and A.S. Jensen, *Phys.Lett. B* **600**, 208-214 (2004).
- [19] E. Garrido, D.V. Fedorov and A.S. Jensen, *Eur. Phys. J. A* **25** (2005) 365.
- [20] E. Garrido, D.V. Fedorov, A.S. Jensen, H.O.U. Fynbo, *Nucl. Phys. A* **748**, 27 (2005).
- [21] E. Garrido, D.V. Fedorov, A.S. Jensen and H.O.U. Fynbo, *Nucl.Phys.A* **766** (2005) 74-96.
- [22] E. Garrido, D.V. Fedorov, A.S. Jensen and H.O.U. Fynbo, *Nucl.Phys. A* **748**, 27-38 (2005).
- [23] E. Garrido, D.V. Fedorov, A.S. Jensen and H.O.U. Fynbo, *Nucl.Phys. A* **748**, 39-58 (2005).
- [24] E. Garrido, D.V. Fedorov and A.S. Jensen, *Eur. Phys. J. A* **25**, 365-378 (2005).
- [25] E. Garrido, D.V. Fedorov, A.S. Jensen and H.O.U. Fynbo, *Nucl. Phys. A* **766**, 74 (2006).
- [26] E. Garrido, D.V. Fedorov and A.S. Jensen, *Phys. Rev. Lett.* **96**, 112501 (2006).
- [27] R. de Diego, E. Garrido, D.V. Fedorov, A.S. Jensen, *Nucl. Phys. A* **786** (2007) 71-89.
- [28] E. Garrido, D.V. Fedorov, H.O.U. Fynbo and A.S. Jensen, *Nucl. Phys. A* **781** (2007) 387.
- [29] E. Garrido, D.V. Fedorov, H.O.U. Fynbo and A.S. Jensen, *Phys. Lett. B* **648** (2007) 274-278.

- [30] R. Alvarez-Rodriguez, E. Garrido, A.S. Jensen, D.V. Fedorov, and H.O.U. Fynbo, *Phys.Rev.Lett.* **99**, (2007) 072503
- [31] R. Álvarez-Rodríguez, E. Garrido, A.S. Jensen, D.V. Fedorov, and H.O.U. Fynbo, *Eur. Phys. J. A* **31**, 303 (2007).
- [32] R. Álvarez-Rodríguez, E. Garrido, A.S. Jensen, D.V. Fedorov and H.O.U. Fynbo, *Eur. Phys. J. A* **31**, 303 (2007).
- [33] R. de Diego, E. Garrido, D.V. Fedorov, A.S. Jensen, *Phys. Rev. C* **77** , 024001(10p) (2008).
- [34] R. Alvarez-Rodriguez, E. Garrido, A.S. Jensen, D.V. Fedorov, and H.O.U. Fynbo, *J. Phys. G* **35** (2008) 014010.
- [35] R. Álvarez-Rodríguez, A.S. Jensen, E. Garrido, D.V. Fedorov, H.O.U. Fynbo, *Int.J.Mod.Phys. E* **17** (2008) no. 10.
- [36] E. Garrido, A.S. Jensen and D.V. Fedorov, *Phys.Rev. C* **78** (2008) 034004.
- [37] C. Romero-Redondo, E. Garrido, D.V. Fedorov and A.S. Jensen, *Phys. Lett. B* **660** (2008) 32-36.
- [38] C. Romero-Redondo, E. Garrido, D.V. Fedorov and A.S. Jensen, *Phys. Rev. C* **77** (2008) 054313 (1-15).
- [39] R. Álvarez-Rodríguez, A.S. Jensen, E. Garrido, D.V. Fedorov and H.O.U. Fynbo, *Phys. Rev. C* **77** 064305 (2008).
- [40] R. Álvarez-Rodríguez, H.O.U. Fynbo, A.S. Jensen and E. Garrido, *Phys. Rev. Lett.* **100**, 192501 (2008).

- [41] H.O.U. Fynbo, R. Álvarez-Rodríguez, A.S. Jensen, O.S. Kirsebom and D.V. Fedorov, *Phys. Rev. C* **79**, 054009 (2009).
- [42] R. Álvarez-Rodríguez, A.S. Jensen, E. Garrido, D.V. Fedorov, H.O.U. Fynbo, O.S Kirsebom, *Few-Body Systems* **45** (2009) 149-152.
- [43] D.V. Fedorov, A.S. Jensen, M. Thøgersen, E. Garrido, and R. de Diego, *Few-Body Systems* **45** (2009) 191-195.
- [44] E. Garrido, A.S. Jensen and D.V. Fedorov, *Phys. Lett. B* **684**, 132 (2010).
- [45] R. de Diego, E. Garrido, D.V. Fedorov, A.S. Jensen, *Europhys. Lett.*, **90** (2010) 52001.
- [46] R. de Diego, E. Garrido, D.V. Fedorov, A.S. Jensen, *J.Phys.Conf.Series* **205** (2010) 01204.
- [47] R. Álvarez-Rodríguez, A.S. Jensen, E. Garrido, D.V. Fedorov  
Structure and three-body decay of  $^9\text{Be}$  resonances *Phys. Rev. C* **82** (2010) 034001
- [48] A.S. Jensen, D.V. Fedorov, E. Garrido, *J. Phys.G* **37** (2010) 064027.
- [49] C. Aa. Diget et al., *Nucl. Phys.A* **760** (2005) 3.
- [50] C. Aa. Diget, Phd-thesis, Aarhus University.